Behavior of tropopause height and atmospheric temperature in models, reanalyses, and observations: Decadal changes

B. D. Santer,[1] R. Sausen,[2] T. M. L. Wigley,[3] J. S. Boyle,[1] K. AchutaRao,[1] C. Doutriaux,[1] J. E. Hansen,[4] G. A. Meehl,[3] E. Roeckner,[5] R. Ruedy,[4] G. Schmidt,[4] and K. E. Taylor[1]

Received 1 March 2002; revised 21 June 2002; accepted 24 June 2002; published 3 January 2003.

[1] We examine changes in tropopause height, a variable that has hitherto been neglected in climate change detection and attribution studies. The pressure of the lapse rate tropopause, p_{LRT}, is diagnosed from reanalyses and from integrations performed with coupled and uncoupled climate models. In the National Centers for Environmental Prediction (NCEP) reanalysis, global-mean p_{LRT} decreases by 2.16 hPa/decade over 1979–2000, indicating an increase in the height of the tropopause. The shorter European Centre for Medium-Range Weather Forecasts (ECMWF) reanalysis has a global-mean p_{LRT} trend of −1.13 hPa/decade over 1979–1993. Simulated p_{LRT} trends over the past several decades are consistent with reanalysis results. Superimposed on the overall increase in tropopause height in models and reanalyses are pronounced height decreases following the eruptions of El Chichón and Pinatubo. Interpreting these p_{LRT} results requires knowledge of both $T(z)$, the initial atmospheric temperature profile, and $\Delta T(z)$, the change in this profile in response to external forcing. $T(z)$ has a strong latitudinal dependence, as does $\Delta T(z)$ for forcing by well-mixed greenhouse gases and stratospheric ozone depletion. These dependencies help explain why overall tropopause height increases in reanalyses and observations are amplified toward the poles. The pronounced increases in tropopause height in the climate change integrations considered here indicate that even AGCMs with coarse vertical resolution can resolve relatively small externally forced changes in tropopause height. The simulated decadal-scale changes in p_{LRT} are primarily thermally driven and are an integrated measure of the anthropogenically forced warming of the troposphere and cooling of the stratosphere. Our algorithm for estimating p_{LRT} (based on a thermal definition of tropopause height) is sufficiently sensitive to resolve these large-scale changes in atmospheric thermal structure. Our results indicate that the simulated increase in tropopause height over 1979–1997 is a robust, zero-order response of the climate system to forcing by well-mixed greenhouse gases and stratospheric ozone depletion. At the global-mean level, we find agreement between the simulated decadal-scale p_{LRT} changes and those estimated from reanalyses. While the agreement between simulated p_{LRT} changes and those in NCEP is partly fortuitous (due to excessive stratospheric cooling in NCEP), it is also driven by real pattern similarities. Our work illustrates that changes in tropopause height may be a useful "fingerprint" of human effects on climate and are deserving of further attention. *INDEX TERMS:* 1610 Global Change: Atmosphere (0315, 0325); 1620 Global Change: Climate dynamics (3309); 3362 Meteorology and Atmospheric Dynamics: Stratosphere/troposphere interactions; 8409 Volcanology: Atmospheric effects (0370); *KEYWORDS:* tropopause height, tropospheric temperatures, stratospheric temperatures, climate modeling, microwave sounding unit

Citation: Santer, B. D., et al., Behavior of tropopause height and atmospheric temperature in models, reanalyses, and observations: Decadal changes, *J. Geophys. Res.*, *108*(D1), 4002, doi:10.1029/2002JD002258, 2003.

[1]Program for Climate Model Diagnosis and Intercomparison, Lawrence Livermore National Laboratory, Livermore, California, USA.
[2]Institut für Physik der Atmosphäre, Deutsches Zentrum für Luft- und Raumfahrt, Oberpfaffenhofen, Wessling, Germany.
[3]National Center for Atmospheric Research, Boulder, Colorado, USA.
[4]NASA Goddard Institute for Space Studies, New York, New York, USA.
[5]Max-Planck Institute for Meteorology, Hamburg, Germany.

Copyright 2003 by the American Geophysical Union.
0148-0227/03/2002JD002258$09.00

1. Introduction

[2] In 1996, the Intergovernmental Panel on Climate Change (IPCC) concluded that [*Houghton et al.*, 1996, p. 4] "the balance of evidence suggests a discernible human influence on global climate." The latest IPCC report reinforces this conclusion, and finds that [*Houghton et al.*, 2001, p. 10] "most of the observed warming over the last 50 years is likely to have been due to the increase in

greenhouse gas concentrations.'' These statements are based on multiple lines of evidence. One line of evidence is from formal statistical studies that seek to identify model-predicted ''fingerprints'' of anthropogenic effects in observational climate records [*Santer et al.*, 1996a; *Mitchell et al.*, 2001].

[3] To date, this work has focused on either surface temperature [*Santer et al.*, 1995; *Hegerl et al.*, 1996, 1997; *Wigley et al.*, 1998; *Tett et al.*, 1999; *Stott et al.*, 2000; *Allen et al.*, 2002] or on zonally averaged temperatures in the free atmosphere [*Karoly et al.*, 1994; *Santer et al.*, 1996b; *Tett et al.*, 1996]. The case for a discernible human influence on global climate would be strengthened by successful ''fingerprint'' studies of variables other than surface temperature or zonal-mean temperature profiles. A global-scale human-induced climate change signal should be manifest in a variety of climate variables, and not in temperature alone.

[4] Examples of statistical studies using alternative detection variables include analyses of changes in integrated ocean heat content [*Barnett et al.*, 2001] and Northern Hemisphere sea ice extent [*Vinnikov et al.*, 1999]. There has also been interest in various temperature-related indices, such as the temperature contrast between land and ocean, low and high latitudes, and the Northern and Southern Hemispheres [*Karoly and Braganza*, 2001]. Other indices, such as the ''Greenhouse Climate Response Index'' of *Karl et al.* [1996] and the ''Common-Sense Climate Index'' of *Hansen et al.* [1998], simultaneously consider changes in temperature and moisture. This body of work suggests that a coherent human-induced climate change signal is emerging in a number of different variables, and is not limited to temperature only.

[5] One variable that has not been examined from a climate change standpoint is the height of the tropopause. The tropopause is the transition zone between the turbulently mixed troposphere and the more stably stratified stratosphere [*Hoinka*, 1998]. This transition is also marked by changes in lapse rate and the chemical composition of the atmosphere. Thus the location of the tropopause can be defined in a variety of ways, according to dynamic, thermal, and chemical properties of the atmosphere [*Hoinka*, 1998; *Seidel et al.*, 2001].

[6] Various studies have attempted to elucidate the key factors that determine the latitude-altitude distribution of the tropopause [*Held*, 1982; *Thuburn and Craig*, 1997; *Haynes et al.*, 2001]. Initial investigations were based on radiosonde data [*Reid and Gage*, 1984, 1985]. More recently, analyses from numerical weather prediction centers [*Reichler et al.*, 1996] and ''reanalysis'' products [*Hoinka*, 1998; *Randel et al.*, 2000] have provided insights into the climatological properties of the tropopause, its seasonal cycle, and its secular variations on interannual and decadal timescales. Much of this work has been summarized by *Seidel et al.* [2001]. It reveals that the tropopause responds to a variety of influences, such as variations in solar radiation [*Reid and Gage*, 1981], atmospheric angular momentum [*Reid and Gage*, 1984], stratospheric ozone [*Dameris et al.*, 1995; *Hoinka*, 1998], and explosive volcanic eruptions [*Reid and Gage*, 1985; *Randel et al.*, 2000].

[7] There have been few model-based studies of tropopause height. *Thuburn and Craig* [1997, 2000] used an atmospheric General Circulation Model (GCM) to test different theories regarding the key factors determining tropopause height. They found the simulated tropopause height to be sensitive to surface temperature (through changes in the atmospheric moisture distribution), somewhat less sensitive to the distribution of ozone and changes in the equator-to-pole temperature gradient, and relatively insensitive to changes in the Earth's rotation rate. Since these experiments were performed in perpetual January mode, possible controls on decadal-timescale changes in tropopause height could not be examined.

[8] A number of observational studies have identified decadal-timescale changes in tropopause height. A useful review is given by *Ramaswamy et al.* [2001]. Virtually all of these studies show an increase in the height of the tropopause over the last several decades or longer, either at individual radiosonde stations [*Steinbrecht et al.*, 1998], networks of stations in the tropics [*Seidel et al.*, 2001], or in tropical averages from reanalysis products [*Randel et al.*, 2000]. One obvious question is whether similar changes occur in climate model experiments driven by estimates of historical changes in natural and anthropogenic forcings.

[9] *Ramaswamy et al.* [2001] suggest that the poor vertical resolution of most current climate models precludes their simulation of multi-decadal changes in tropopause height. To test this assumption, we investigate tropopause height changes in climate change experiments performed with two different coupled atmosphere-ocean GCMs [*Roeckner et al.*, 1999; *Hansen et al.*, 2002]. We find that despite relatively coarse vertical resolution, both models show similar decadal-scale increases in tropopause height in response to anthropogenic forcing.

[10] To gain insights into the possible controls on low-frequency changes in tropopause height, we examine its behavior in control integrations and in climate change experiments with different combinations of anthropogenic and natural forcings. The forcings that we focus on are changes in well-mixed greenhouse gases, stratospheric and tropospheric ozone, volcanic aerosols, and direct and indirect sulfate aerosol effects. Variations in these constituents (either individually or jointly) can yield markedly different temperature responses in the troposphere and stratosphere [*Hansen et al.*, 1997, 2002; *Bengtsson et al.*, 1999]. Such large-scale changes in the static stability of the atmosphere may in turn influence tropopause height. Thus by studying the stratospheric and tropospheric temperature responses to different forcing mechanisms, we can help to elucidate the effects of these forcings on tropopause height. The layer-averaged stratospheric and tropospheric temperatures that we compute here are also a key component of a companion paper (B. D. Santer et al., Behavior of tropopause height and atmospheric temperature in models, reanalyses, and observations: Signal detection, submitted to *Journal of Geophysical Research*, 2002) (hereinafter referred to as Santer et al., submitted manuscript, 2002) which seeks to compare the relative detectability of changes in temperature and tropopause height.

[11] The structure of the present paper is as follows. In section 2, we introduce the model and observational data sets used here and describe the methods employed for calculating layer-averaged temperatures and tropopause pressure. Section 3 gives a brief comparison of the climatological mean

state of tropopause height in model and reanalysis data. The remainder of the paper focuses on decadal-scale changes in tropopause height and layer-averaged atmospheric temperature. Global-mean changes in these variables are compared in section 4. The comparison focuses on the last two decades, although there is also some analysis of simulated changes over the next 50–100 years. In section 5, we examine how greenhouse-gas forcing modifies spatially averaged profiles of atmospheric temperature and affects tropopause height. Horizontal patterns of changes in atmospheric temperature and tropopause height are described in section 6. Simple pattern correlations are used to assess the relative influence of stratospheric and tropospheric temperature fluctuations on tropopause height. Section 7 provides a brief summary and conclusions.

2. Data and Calculation of Derived Variables

2.1. Observational Data

[12] Our temperature data are from the satellite-based MSU instrument, which uses the upwelling microwave radiation from oxygen molecules to estimate the vertically weighted temperature of deep atmospheric layers [*Spencer and Christy*, 1990]. Most interest in MSU temperatures has focused on products for the stratosphere, mid- to upper troposphere, and lower troposphere. These are monitored by (respectively) MSU channels 4 and 2, and by the lower tropospheric retrieval (2LT). The MSU weighting functions for these three layers peak at 74, 595, and 740 hPa.

[13] We rely on version d of the MSU data [*Christy et al.*, 2000]. Data were available as monthly means for 2.5° × 2.5° latitude/longitude gridboxes. They have full global coverage and span the 264-month period January 1979 through December 2000.

[14] We obtain estimates of "observed" tropopause pressure and equivalent MSU temperatures from reanalysis projects, which involve use of an atmospheric numerical weather forecast model with a fixed observational data assimiliation system. We employ data from two reanalyses. The first was jointly performed by the National Centers for Environmental Prediction (NCEP) and the National Center for Atmospheric Research (NCAR) [*Kalnay et al.*, 1996]. The second was conducted by the European Centre for Medium-Range Weather Forecasts (ECMWF) [*Gibson et al.*, 1997]. We refer to these reanalyses subsequently as "NCEP" and "ERA."

[15] Detailed descriptions of these data sets are given elsewhere [*Pawson and Fiorino*, 1998; *Santer et al.*, 1999]. Here, it is sufficient to note that the operational models had different horizontal resolution (T62 for NCEP versus T106 for ERA), but similar vertical resolution (17 pressure levels). Sixteen of these 17 levels are identical (10, 30, 50, 70, 100, 150, 200, 250, 300, 400, 500, 600, 700, 850, 925 and 1000 hPa). NCEP has a pressure level at 20 hPa that is absent in ERA, while ERA has a 775 hPa level that is not present in NCEP. To facilitate comparison of the reanalyses, they were interpolated to a common 2.5° × 2.5° latitude/longitude grid.

[16] The NCEP data extend from January 1948 through December 2000. We did not use NCEP temperatures prior to January 1979 due to well-documented inhomogeneities that exist around the time of transition to satellite data assimilation [*Pawson and Fiorino*, 1998; *Santer et al.*, 1999; *Randel et al.*, 2000]. The ERA reanalysis does not span this transition period, and extends from January 1979 through February 1994. Even after 1979, however, it is likely that climate records from both reanalyses incorporate discontinuities related to biases in the assimilated satellite data [*Trenberth et al.*, 2001].

2.2. Model Data

[17] We used model data from three sources: the Max-Planck Institute for Meteorology in Hamburg (MPI), NCAR, and the Goddard Institute for Space Studies (GISS). The models and integrations in question have been described in detail elsewhere [*Roeckner et al.*, 1996, 1999; *Bengtsson et al.*, 1999; *Washington et al.*, 2000; *Meehl et al.*, 2000; *Hansen et al.*, 2002; *Santer et al.*, 2001].

[18] The MPI data were from experiments performed with the ECHAM4 atmospheric GCM coupled to an isopycnal ocean model (OPYC; *Oberhuber* [1993]). The ECHAM4 model was jointly developed by MPI and the Meteorological Institute of the University of Hamburg on the basis of an ECMWF forecast model. The AGCM was run at T42 spectral truncation and has a 19-level hybrid sigma-pressure coordinate system, with the top of the model atmosphere at 10 hPa. Temperature data used in the calculation of tropopause height were archived at 15 discrete pressure levels (30, 50, 70, 100, 150, 200, 250, 300, 500, 600, 700, 850, 900, 950, and 1000 hPa). The OPYC ocean component has comparable horizontal resolution to the atmosphere poleward of 36°, with gradually decreasing meridional grid spacing equatorward of 36°, down to 0.5° at the equator. OPYC has 11 vertical layers.

[19] In the present study, we analyze six different ECHAM4/OPYC integrations. The baseline integration, GHG, has time-dependent changes in well-mixed greenhouse gases. It commences in 1860 and ends in 2099. Other forcings are added sequentially to the baseline case. The additional forcings are the direct scattering effects of sulfate aerosols (GSD), indirect aerosol effects and tropospheric ozone changes (GSDIO), stratospheric ozone depletion (GSO1, GSO2), and stratospheric aerosols from the June 1991 eruption of Mount Pinatubo (GSOP). Full details of the forcings are given by *Roeckner et al.* [1999] and *Bengtsson et al.* [1999].

[20] GSD and GSDIO start in 1860 and extend to 2050, while GSOP, GSO1 and GSO2 span the 228-month period from January 1979 through December 1997. The GSO1 and GSO2 experiments use January 1979 oceanic initial conditions from GSDIO. GSO1 and GSO2 have the same forcing, but start from slightly different atmospheric initial conditions in January 1979. GSOP's initial conditions were taken from June 1991 in GSO1. We also analyzed ECHAM4/OPYC data from a 300-year control integration with no changes in natural or anthropogenic forcings.

[21] In addition to the ECHAM control run, we also considered data from a 300-year control integration performed with the Parallel Climate Model (PCM) jointly developed by NCAR and the Los Alamos National Laboratory [*Washington et al.*, 2000]. The atmospheric component of PCM is version 3 of NCAR's Community Climate Model (CCM3; *Boville and Hurrell* [1998]) with a T42 spectral truncation (roughly 2.8° × 2.8° horizontal resolu-

tion) and 18 vertical levels. The PCM ocean component has 32 vertical levels and 2/3° × 2/3° horizontal resolution, decreasing to 0.5° at the equator.

[22] Our use of PCM data provides a second model-based estimate of the natural internal variability of tropopause height and atmospheric temperature. We employ this information to assess whether the externally forced signals in these variables are large relative to their unforced variability (section 4.3). The PCM variability estimates are also a key component of the optimal detection scheme used by Santer et al. (submitted manuscript, 2002).

[23] A key result of our study is that there are pronounced tropopause height signals in climate change experiments performed with the ECHAM model (section 4.3). To investigate the model dependence of this finding, we examine tropopause height changes simulated by the GISS SI2000 AGCM [*Hansen et al.*, 2002]. Our analysis of GISS climate change simulations is limited to global-mean tropopause height data only. We stress that it serves primarily as an independent check on the tropopause height signals estimated from ECHAM.

[24] The GISS SI2000 AGCM has coarser horizontal and vertical resolution (4° × 5° latitude/longitude and 12 vertical layers) than either ECHAM or PCM. The AGCM employs sigma coordinates up to 150 hPa, and pressure coordinates above 150 hPa, with discrete pressure level boundaries at 10, 30, 60, 100, 150, 210, 285, 390, 550, 720, 854, 934, and 984 hPa. We used a model version with 2nd order differencing in the momentum equation. In the experiments considered here, the SI2000 AGCM was driven by prescribed, time-varying changes in observed sea surface temperatures (SSTs) and sea ice, as well as by combined temporal variations in well-mixed greenhouse gases, volcanic aerosols, solar irradiance, ozone, stratospheric water vapor, and tropospheric aerosols [*Hansen et al.*, 2002]. There are five different realizations of this experiment, each commencing from slightly different atmospheric initial conditions. Although the integrations cover the period 1951–2000, our analysis is restricted to 1979–1997 only to facilitate comparisons with ECHAM. The integrations, forcings, and key physics improvements in the atmospheric model (relative to the GISS SI95 AGCM) are described in detail by *Hansen et al.* [2002].

2.3. Calculation of Derived Variables

[25] To facilitate comparison with the actual MSU temperatures, we used a static global-mean weighting function to compute "equivalent" MSU temperatures from the reanalysis, ECHAM, and PCM data. This procedure is described by *Santer et al.* [1999]. For global and hemispheric means, the static weighting function results are very similar to those obtained with a full radiative transfer code.

[26] We use the thermal definition of the tropopause here, also referred to as the lapse rate tropopause (LRT) [*Hoinka*, 1998; *Seidel et al.*, 2001]. The thermal tropopause has been defined by the World Meteorological Organization (WMO) as [*World Meteorological Organization* (*WMO*), 1957, p. 137] "the lowest level at which the lapse rate decreases to 2°C/km or less, provided also the average lapse rate between this level and all higher levels within 2 km does not exceed 2°C/km." Relative to other definitions of the tropopause, such as those based on potential vorticity (PV), the thermal definition has the advantage that it is easily computed from sigma-level or pressure-level temperature data. The PV-defined tropopause height cannot be computed close to the equator and depends on the (somewhat arbitrary) choice of the threshold PV value [*Hoinka*, 1998]. The LRT has the disadvantage that it is sometimes difficult to compute at very high latitudes, for reasons discussed by *Reichler et al.* [1996].

[27] The algorithms used to derive LRT [cf. *Reichler et al.*, 1996; *Hoinka*, 1998] are typically applied using linear interpolation of the lapse rate in a p^{κ}-coordinate system, where p denotes pressure, $\kappa = R/c_p$, and R and c_p are the gas constant for dry air and the specific heat capacity of dry air at constant pressure. Differences between algorithms relate to the number of levels involved in the interpolation. *Hoinka* [1998] identifies the model level that first satisfies the WMO criterion, and then computes the mean lapse rates of the four layers above and below the two "central layers" surrounding the threshold level. He defines the pressure of the LRT (henceforth p_{LRT}) as the point at which the mean lapse rates intersect. In contrast, the interpolation by *Reichler et al.* [1996] relies only on the layers immediately above and below the threshold level.

[28] We use the *Reichler et al.* [1996] algorithm here, and apply this to ECHAM, PCM, and reanalysis data sets. At each grid-point, we calculate p_{LRT} from the monthly mean temperature profile at discrete pressure levels. Our justification for the use of monthly mean data to compute p_{LRT} is discussed in Appendix A. Global-mean p_{LRT} values for the GISS climate change experiments were also computed with the WMO criterion, using an algorithm very similar to that of *Reichler et al.* [1996].

3. Climatological-Mean Tropopause Height

[29] Our focus here is on studying decadal-scale changes in p_{LRT}, and on identifying the key forcings that may be responsible for such changes. In the following, we provide only a brief comparison of the mean state of p_{LRT} in model and reanalysis data.

[30] Meridional profiles of zonally and annually averaged p_{LRT} are shown in Figure 1 for the reanalyses, ECHAM, and PCM. All have a higher tropopause in the tropics and subtropics, a much lower tropopause toward the poles, and steep gradients in tropopause pressure between the subtropics and high latitudes [cf. *Hoinka*, 1998].

[31] The NCEP and ERA results are very similar except at mid- to high latitudes in the Southern Hemisphere, where radiosonde coverage is sparse and the reanalyses are poorly constrained by observations. PCM's tropopause is consistently lower than in both reanalyses between roughly 25°N–25°S. In contrast, ECHAM's tropopause is higher than in NCEP and ERA between approximately 20°N–20°S. In the vicinity of the subtropical jets, ECHAM's p_{LRT} errors are larger than those in PCM, which may reflect a smaller cold bias in PCM. ECHAM overestimates tropopause height poleward of 40° in both hemispheres. PCM shows similar but less pronounced errors.

[32] The differences between simulated zonal-mean p_{LRT} values and those in NCEP and ERA generally exceed the differences between the reanalyses themselves. Model-ver-

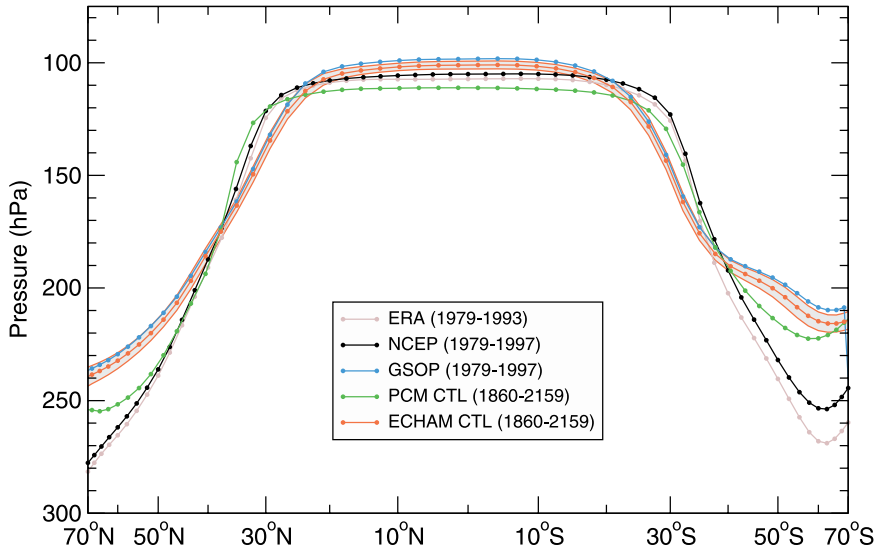

Figure 1. Zonal-mean annual-mean p_{LRT} in reanalyses and model integrations. The averaging periods are listed in the legend. p_{LRT} values are not shown poleward of 70° due to difficulties in defining p_{LRT} at high latitudes [*Reichler et al.*, 1996]. The grey shading marks the ±2σ limits for the ECHAM control run p_{LRT} values. It is a measure of how p_{LRT} varies due to (simulated) interannual variability. The interannual variability in p_{LRT} for PCM (not shown) is similar to that of ECHAM.

sus-reanalysis discrepancies cannot be explained by external forcing alone, since they are larger than the p_{LRT} differences between the ECHAM control run and the GSOP experiment. They are also larger than the uncertainties in estimates of the simulated mean state arising from interannual variability in p_{LRT} (see grey shading in Figure 1).

[33] Note that p_{LRT} was estimated from ECHAM, PCM, and reanalysis datasets in which the vertical resolution was similar (section 2). We infer from this that the differences between simulated climatological mean p_{LRT} values and those in NCEP and ERA are not simply due to overall vertical resolution, and likely reflect both resolution differences in the vicinity of the tropopause and systematic model errors, such as cold biases in the vicinity of the polar night jets [*Gates et al.*, 1999].

4. Global-Mean Changes

4.1. Time Series

[34] We begin by examining global-mean monthly mean anomaly time series of p_{LRT} and layer-averaged atmospheric temperature. Our focus is on January 1979 through December 1997, the period covered by the three ECHAM experiments most relevant for comparison with observations and reanalyses (GSO1, GSO2, and GSOP). We also present some observational and reanalysis results for the longer period January 1979 through December 2000.

4.1.1. Lapse Rate Tropopause

[35] In the NCEP reanalysis, the most prominent feature of the global-mean p_{LRT} data is a decrease in tropopause pressure of 2.16 hPa/decade over 1979–2000, corresponding to an increase in the height of the tropopause. Superimposed on this overall trend is higher-frequency variability, part of which is associated with the eruptions of El Chichón and Pinatubo (Figure 2a). Values of p_{LRT} increase after both eruptions, indicating a lower tropopause altitude. The maximum increase after Pinatubo is larger than after El Chichón, consistent with the larger estimated forcing of Pinatubo [*Hansen et al.*, 1997, 2002; *Andronova et al.*, 1999; *Santer et al.*, 2001; T. M. L. Wigley and B. D. Santer, Differential ENSO and volcanic effects on surface and tropospheric temperatures, submitted to *Journal of Climate*, 2002] (hereinafter referred to as Wigley and Santer, submitted manuscript, 2002). It is evident that the volcanically induced p_{LRT} signals persist for at least several years.

[36] Values of p_{LRT} also show overall decreases in the ECHAM and GISS climate change experiments (Figures 2b and 2c). Consider the ECHAM results first. In GSO1, GSO2, and GSOP, the linear trends in p_{LRT} over 1979–1997 are −2.43, −1.94, and −1.47 hPa/decade (respectively). The p_{LRT} trend in NCEP over the same time period is −1.82 hPa/decade. GSO1 and GSO2 have larger negative trends than NCEP due to their neglect of the p_{LRT} increases caused by El Chichón and Pinatubo. GSOP has a smaller negative trend than NCEP due to its neglect of El Chichón and its slightly larger p_{LRT} increase after Pinatubo. Inclusion of El Chichón's effects in GSOP would yield a larger negative trend in p_{LRT}, bringing GSOP in better agreement with the NCEP result. At the global-mean level, the decay time of the p_{LRT} response to Pinatubo is similar in GSOP and the reanalyses (Figure 2d).

[37] In the five realizations of the GISS climate change experiment, p_{LRT} trends over 1979–1997 range from −1.30 to −1.52 hPa/decade (Figure 2c). The trend in the ensemble-mean of the GISS p_{LRT} data is −1.40 hPa/decade. None of the GISS trend results is significantly different from the NCEP p_{LRT} trend of −1.82 hPa/decade, although all are smaller (i.e., less negative). The latter result is due (at least in part) to the larger Pinatubo signal in GISS than in NCEP (Figure 2d). These differences in the GISS and NCEP p_{LRT} responses to Pinatubo eruption may be driven by pro-

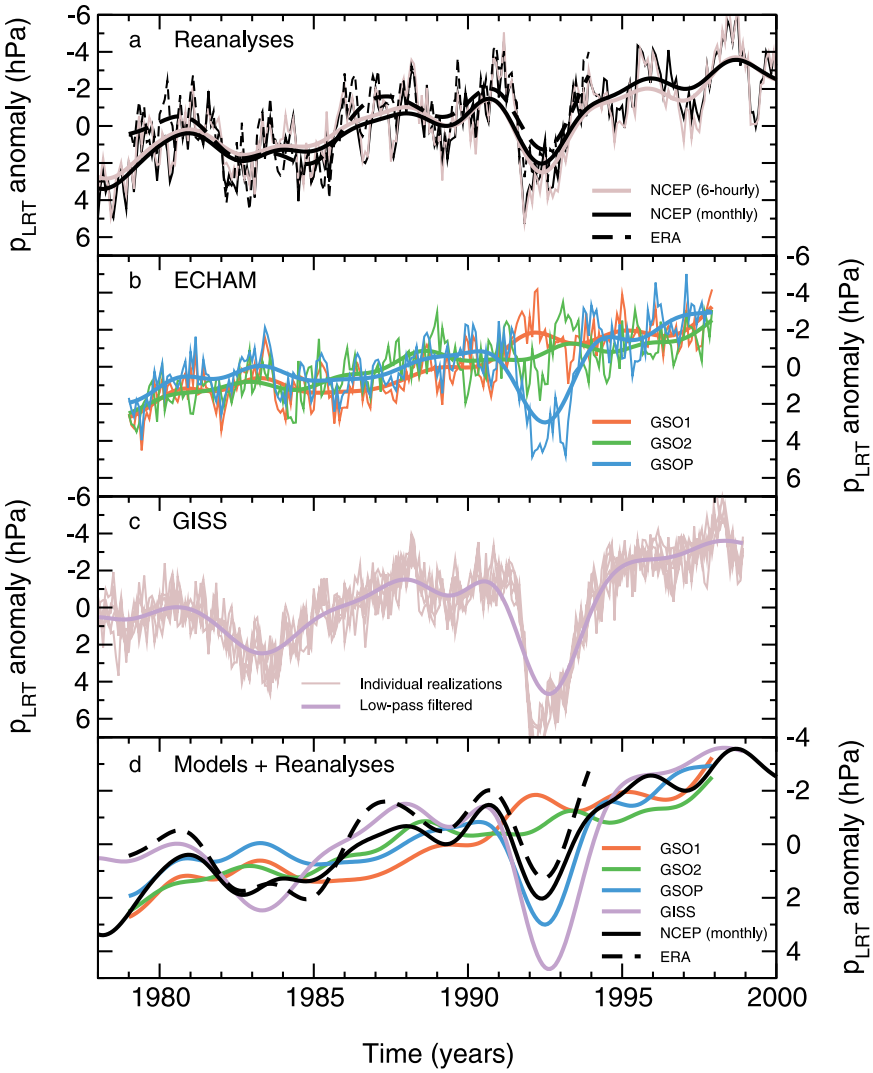

Figure 2. Time series of global-mean monthly mean changes in p_{LRT}, the pressure of the lapse rate tropopause, in reanalyses (panel a) and model experiments performed with the ECHAM and GISS models (panels b and c, respectively). A decrease in p_{LRT} signifies an increase in the height of the tropopause. For sources of data, refer to section 2. The top three panels show both low-pass filtered and unfiltered results (bold and thin lines, respectively). The bottom panel (panel d) compares low-pass filtered results in models and reanalyses. Data are expressed as anomalies relative to climatological monthly means over 1979 to 1997 (1979 to 1993 for ERA). Low-pass filtering uses the SMOOFT routine of *Press et al.* [1986].

nounced differences in both the vertical and the meridional structure of the atmospheric temperature changes after Pinatubo.

[38] Tropical p_{LRT} data also show an overall decrease in tropopause pressure in both reanalyses and the ECHAM experiments (Figure 3). The decreases are consistently smaller in the tropics than in the globally averaged data: tropical p_{LRT} trends in GSO1, GSO2, GSOP, and NCEP over 1979–1997 are −1.65, −1.50, −0.34, and −1.05 hPa/decade, respectively. Possible reasons for the smaller tropical trends are discussed in section 5. As in the case of the global-mean data, GSO1 and GSO2 have larger negative trends than NCEP due to their neglect of volcanic effects on p_{LRT}. GSOP has a much smaller negative trend than NCEP due to the unrealistically large tropical response to Pinatubo in the model experiment and the neglect of El Chichón. While NCEP's response is roughly 20% smaller in the tropics than in the global average, the converse is the case for GSOP: the tropical response is about 70% larger than the global-mean response.

[39] Several previous studies provide useful checks on our estimates of p_{LRT} changes in the NCEP and ERA reanalyses. *Seidel et al.* [2001], using three different networks of radiosonde stations located between 15°N–15°S, found least-squares linear trends in p_{LRT} of roughly −0.6 to −0.8 hPa/decade over the period 1978–1997. To facilitate comparison with Seidel et al., we averaged NCEP p_{LRT} data over the same latitude band. Our estimated trend over 1978–1997, −0.68 hPa/decade, is consistent with Seidel et al.'s results.

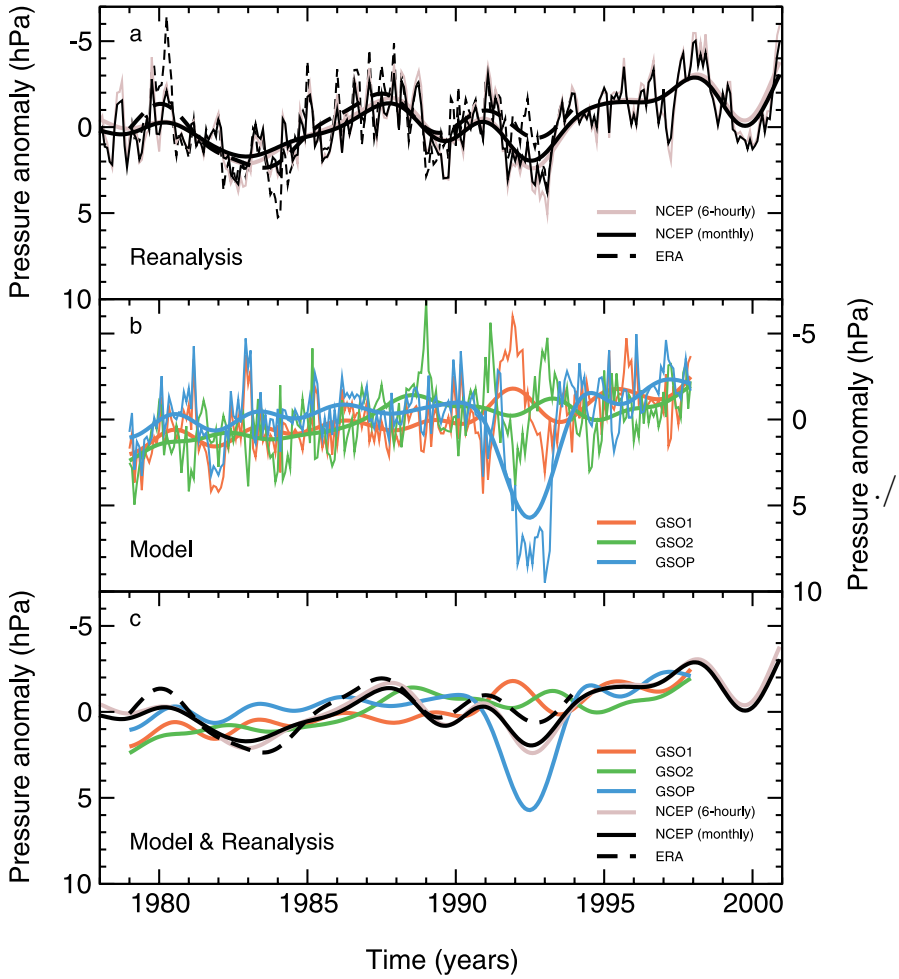

Figure 3. As for Figure 2, but for p_{LRT} values averaged over 30°N–30°S.

[40] In contrast, *Randel et al.* [2000] obtain a smaller trend (−0.32 hPa/decade over 1979–1997) using NCEP-based estimates of p_{LRT} averaged over 20°N–20°S. Our estimate of the NCEP trend over the same area and time period is larger than this (−0.74 hPa/decade) and is in better accord with the *Seidel et al.* [2001] results.

[41] A further reference point is the study by *Hoinka* [1998], who calculated p_{LRT} from ERA. Hoinka's estimate of the global-mean trend in p_{LRT} (−0.1 hPa/decade over 1979–1993) is an order of magnitude smaller than our own estimate from the same data (−1.13 hPa/decade). This discrepancy may be related to the differences in the algorithms used to determine p_{LRT} (see section 2.3). We note that our result for ERA is in very good agreement with our estimate of the global-mean p_{LRT} trend in the NCEP data (−1.05 hPa/decade over 1979–1993).

4.1.2. Lower Stratospheric Temperature

[42] Lower stratospheric temperatures in actual MSU data and reanalyses are characterized by pronounced decreases in temperature over the satellite era (Figure 4a). Some portion of this multidecadal cooling is attributable to the combined effects of stratospheric ozone depletion and increases in well-mixed greenhouse gases [*Ramaswamy et al.*, 1996, 2001]. Superimposed on the overall cooling of the lower stratosphere are the prominent warming signatures of El Chichón and Pinatubo. The warming results from increased absorption of incoming solar radiation and upwelling terrestrial infrared radiation by volcanic aerosols [*Ramaswamy et al.*, 2001].

[43] Note that the linear decrease in stratospheric temperature over 1979–2000 is larger in the NCEP reanalysis than in the actual MSU data (−0.68 versus −0.53°C/decade, respectively). The cooling of NCEP's equivalent channel 4 temperature relative to MSU begins around the time of the Pinatubo eruption, and is sustained through the end of 2000 (Figure 4a). This discrepancy is partly related to NCEP's assimilation of satellite-based temperature retrievals from the National Environmental Satellite Data and Information Service (NESDIS). These retrievals use information from three different satellite-borne instruments, including MSU. Biases and temporal inhomogeneities in the NESDIS retrievals [*Mo et al.*, 1995; *Pawson and Fiorino*, 1998; *Santer et al.*, 1999] and changes in the retrieval algorithm [*Basist and Chelliah*, 1997] contribute to the cooling of NCEP's lower stratosphere relative to MSU. Biases in the radiosonde data assimilated by NCEP may also explain some of the channel 4 trend differences in NCEP and MSU [*Lanzante et al.*, 2002].

[44] The simulated lower stratospheric warming response to Pinatubo in GSOP is roughly twice as large as observed (Figures 4b and 4c). This is partly due to two factors: the model's neglect of the enhanced stratospheric ozone deple-

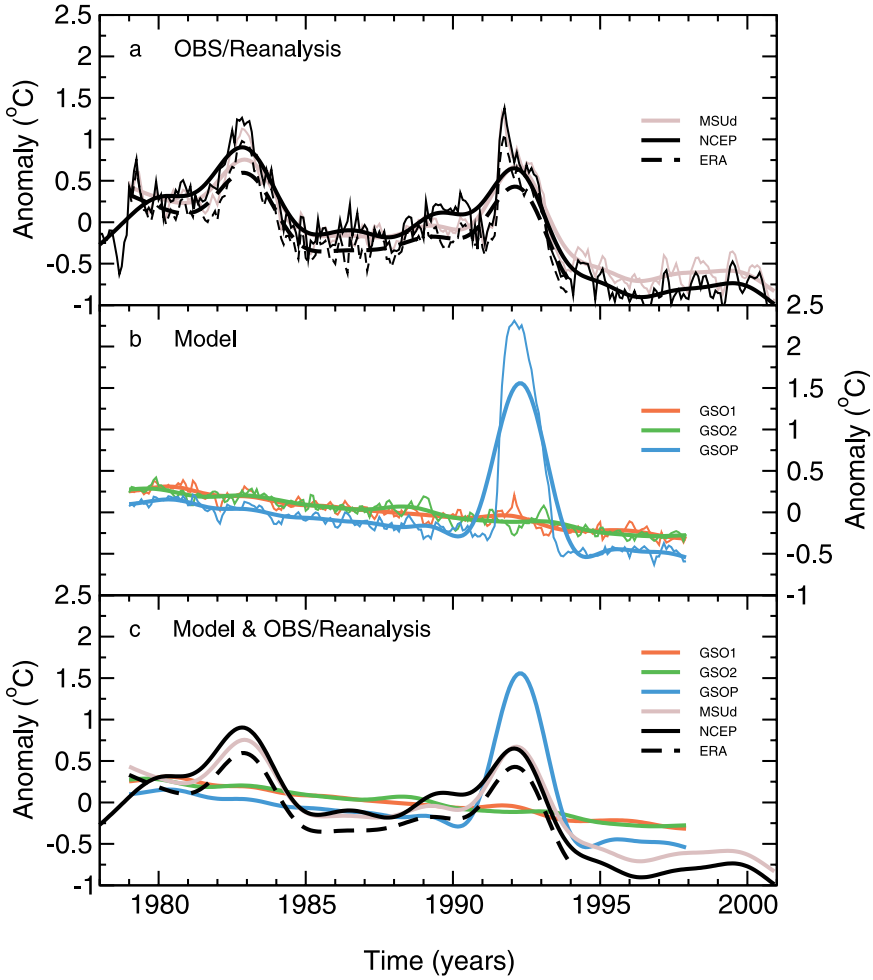

Figure 4. Time series of global-mean monthly mean changes in stratospheric temperatures in observations/reanalyses (panel a) and in ECHAM model experiments (panel b). Sources of data are given in section 2. Results are for actual MSU channel 4 temperatures, and for equivalent channel 4 temperatures computed from the *Bengtsson et al.* [1999] GSO experiments and the NCEP and ERA reanalyses. Panel c compares low-pass filtered results in observations, reanalyses, and model experiments. Refer to Figure 1 for information on filtering and definition of anomalies.

tion caused by Pinatubo, and failure to simulate the equatorial cooling induced by an easterly phase of the quasi-biennial oscillation (QBO) [*Solomon et al.*, 1996; *Bengtsson et al.*, 1999; *Kirchner et al.*, 1999].

4.1.3. Tropospheric Temperature

[45] Mid- to upper tropospheric temperatures (Figure 5) and lower tropospheric temperature (Figure 6) show pronounced warming in the model experiments and virtually no change or a net cooling in the MSU observations and reanalyses. The differences between lower tropospheric temperature trends in MSU and the three GSO experiments are in part related to the effects of volcanic eruptions and ENSO variability. Since the ECHAM experiments were performed with a coupled model (rather than with prescribed SSTs), the phasing of ENSO-induced variability is different in the model and observations. The neglect of volcanic effects (in GSO1 and GSO2) and of El Chichón (in GSOP) also hampers direct model-versus-observed trend comparisons.

[46] *Santer et al.* [2001] and Wigley and Santer (submitted manuscript, 2002) found that statistical removal of volcano and ENSO effects consistently reduced the differences between observed 2LT trends and those simulated by ECHAM, but did not completely reconcile these differences. Remaining discrepancies are probably due to a combination of model error, inaccurate or missing forcings in the model simulations, and observational error [*Wentz et al.*, 2001].

[47] The cooling of NCEP's lower stratospheric temperatures relative to MSU (by −0.15°C/decade; see section 4.1.2) is also evident in channel 2, and to a lesser extent in the 2LT retrieval. The NCEP channel 2 trend over 1979–2000 is negative, while the corresponding trend in the actual MSU data is positive (−0.094 and 0.014°C/decade, respectively). This discrepancy may be partly related to the previously described biases in NCEP's lower stratospheric temperatures. These propagate into the upper troposphere, since channel 2 has a small (roughly 10%) contribution from the lower stratosphere.

4.2. Statistical Significance of Trend Differences

[48] We assess the statistical significance of differences between simulated and observed trends as described by *Santer et al.* [2001]. Our assessment is hampered by the fact

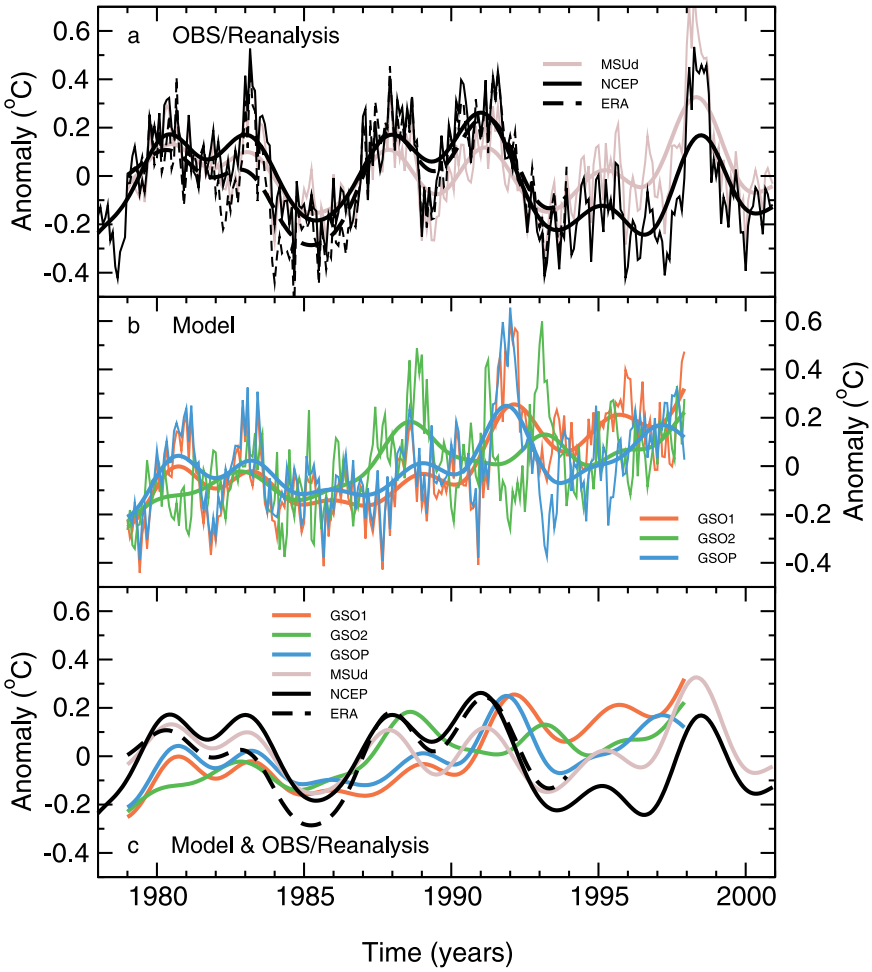

Figure 5. As for Figure 4, but for time series of global-mean monthly mean changes in mid- to upper tropospheric temperatures (MSU channel 2).

that the ECHAM4/OPYC experiments are single realizations (with the exception of GSO1 and GSO2), thus yielding relatively noisy estimates of the underlying responses to the imposed forcings. This problem is exacerbated by the relatively short analysis period: all trend comparisons involve global-mean monthly mean anomaly data over January 1979 to December 1997, the period common to observations and model experiments. (ERA results are excluded since the reanalysis ends in February 1994, and GISS trends will be analyzed elsewhere.) Unforced variability can contribute substantially to short-timescale trends, making it difficult to assess the true trend correspondence between models and observations [*Santer et al.*, 2001]. We compare only "raw" trends here, since our focus is on exploring the effects of different forcings on model/data trend agreement rather than on a comprehensive investigation of trend uncertainties arising from uncertainties in the statistical removal of unforced variability (section 4.1.3).

[49] Except for the GSD experiment, none of the simulated p_{LRT} trends differs significantly from the NCEP p_{LRT} trend (at the 5% level or better; Figure 7a). The model integrations show some correspondence between the magnitude of trends in tropospheric temperature and in p_{LRT}. Larger positive trends in channel 2 and 2LT generally correspond to larger decreases in p_{LRT} (i.e., to larger increases in tropopause altitude). This is why GSD, with the smallest increase in lower tropospheric temperature over 1979–1997, has the smallest increase in tropopause height (compare Figures 7a and 7d).

[50] The model experiments of *Thuburn and Craig* [1997] indicate that p_{LRT} changes are related to variations in stratospheric ozone, presumably through ozone-induced stratospheric temperature changes. Experiments that include stratospheric ozone depletion (GSOP, GSO1, and GSO2) have larger cooling of the lower stratosphere than experiments that do not include this effect (GHG, GSD, and GSDIO; Figure 7b). In general, larger cooling of channel 4 temperatures also leads to a larger decrease in p_{LRT}.

[51] Stratospheric temperature effects explain why GSO1 and GSO2 have the largest decreases in p_{LRT}. Although their tropospheric temperature trends are smaller than in GHG and GSDIO, their stratospheric cooling is considerably larger. p_{LRT} is thus a measure of the integrated response to temperature changes in the troposphere and stratosphere. GSOP, although it includes stratospheric ozone depletion, additionally incorporates the effects of Pinatubo, which increases p_{LRT} (Figure 2b). It therefore has a smaller negative p_{LRT} trend than either GSO1 or GSO2.

[52] Channel 4 cooling trends in all six ECHAM experiments are significantly smaller than in MSU (Figure 7b). As

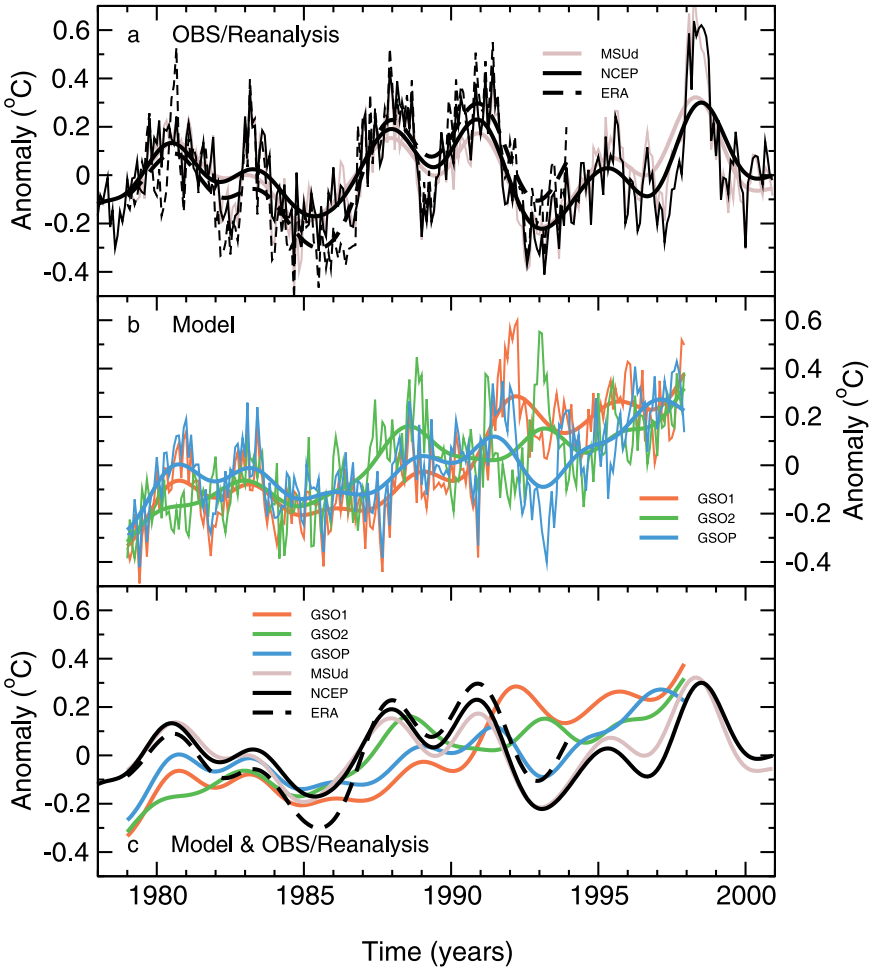

Figure 6. As for Figure 4, but for time series of global-mean monthly mean changes in lower tropospheric temperatures (MSU 2LT retrieval).

noted previously, the GSO1 and GSO2 comparisons have a bias toward increased cooling of the lower stratosphere due to their neglect of volcanically induced stratospheric warming (Figure 4). This is partly offset by a bias toward reduced cooling resulting from the linearized ozone forcing applied by *Bengtsson et al.* [1999].

[53] There are significant differences between the "raw" observed and simulated trends in tropospheric temperature (see *Santer et al.* [2001] and section 4.1.3). This holds for all six experiments, and for both channel 2 and the 2LT retrieval. GSOP, with the most realistic mixture of forcings, yields tropospheric trends closest to those of the actual MSU data.

[54] One puzzling feature of Figure 7 is the relatively close correspondence between the p_{LRT} trends in NCEP and the ECHAM simulations. How can this close agreement occur if tropospheric temperatures over 1979–1997 are cooling in NCEP, yet warming in all model experiments? The agreement may be partly related to stratospheric cooling, which is significantly larger in NCEP than in the actual MSU data or the ECHAM simulations (Figure 7b). This cooling, like the warming of the troposphere, tends to reduce p_{LRT}, and hence compensates for the different behavior of tropospheric temperatures in NCEP and ECHAM. The implication is that the similar global-mean p_{LRT} trends in NCEP and ECHAM may have different relative contributions from temperature changes in the stratosphere and troposphere. We explore this issue further in section 6.

4.3. Simulated Temperature and Tropopause Height Changes on Century Timescales

[55] To gain a better understanding of the factors that influence p_{LRT}, it is useful to examine the evolution of global-mean p_{LRT} and equivalent MSU temperatures in ECHAM simulations of 21st century climate (Figure 8). In the GHG, GSD, and GSDIO experiments, there is an inverse relationship between changes in tropospheric temperature and p_{LRT}: larger increases in temperature lead to larger decreases in p_{LRT} and increases in tropopause height. After roughly 1990, the signals in p_{LRT} and tropospheric temperatures evolve almost linearly and are clearly separated from the natural internal variability of the ECHAM and PCM control runs.

[56] The behavior of stratospheric temperature is more complex (Figure 8b). Equivalent channel 4 temperatures in GHG, GSD, and GSDIO initially decrease from 1860 to present. This is in accord with other model calculations of the expected cooling due to changes in atmospheric CO_2. [*Ramaswamy et al.*, 1996, 2001]. As discussed by *Ramaswamy et al.* [2001], this CO_2-induced cooling is actually the result of two competing effects: increases in both the

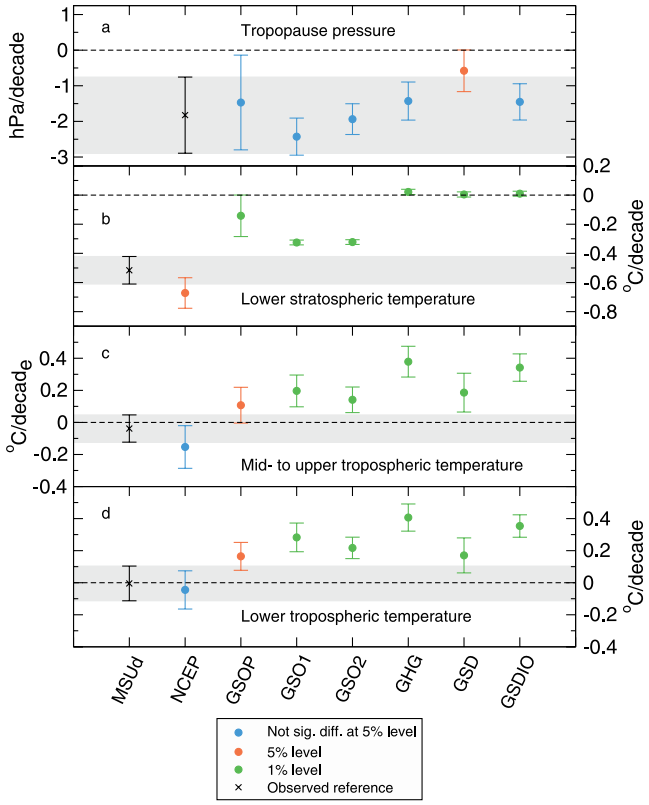

Figure 7. Simulated and observed trends in p_{LRT} (panel a), and in MSU temperatures for channel 4 and 2 and the 2LT retrieval (panels b, c, and d, respectively). Least-squares linear trends are computed over 1979–1997 using global-mean monthly mean anomaly data, with anomalies defined relative to 1979–1997 climatological monthly means. The ±2 σ confidence intervals are also shown. The grey shading denotes the 2 σ confidence intervals for the NCEP p_{LRT} trend and the actual MSU trends. All confidence intervals are adjusted for temporal autocorrelation effects as in *Santer et al.* [2001], with the exception of lower stratospheric temperature trends. The latter have very high lag-1 autocorrelations and small (≤5) effective sample sizes. The statistical significance of differences between modeled trends and observations/reanalysis is assessed as described in section 4.2.

thermal infrared emissivity and the thermal infrared absorptivity of the lower stratosphere (i.e., approximately 50–100 hPa; the region spanning the bulk of the channel 4 weights; see Figure 9). The lower stratosphere is cooled by the former effect and warmed by the latter, and the increased emissivity dominates initially.

[57] After circa 2030, equivalent channel 4 temperatures begin to warm in the GHG, GSD, and GSDIO integrations. There are several explanations for this behavior. The key issue is the shape of the channel 4 weighting function relative to the profile of the emissivity/absorptivity balance, which affects the distribution of cooling and heating in the stratosphere. In the absence of any other factors, trace gas concentration changes would affect stratospheric temperatures through "fast" radiative adjustment, which takes place on timescales of 100 days or less. In reality, this rapid radiative adjustment is convolved with the stratosphere's much slower response to multi-decadal anthropogenic changes in the temperature of the surface and troposphere. This slow CO_2-induced warming of the troposphere leads to increased emission of upwelling longwave radiation, which tends to reduce the initial "fast" radiative cooling of the lower stratosphere [*Forster et al.*, 1997; *Ramaswamy et al.*, 2001].

[58] A second explanation is that the ECHAM climate change experiments explicitly included changes in CH_4, N_2O, CFCs, and HCFCs [*Roeckner et al.*, 1999; *Bengtsson et al.*, 1999]. The radiative effects and horizontal and vertical distributions of these trace gases differ from those of CO_2, both initially and in terms of their changes over time. Calculations with a radiative-convective model show that the lower stratospheric cooling resulting from increases in CO_2 is strongly reduced by additionally including changes in CH_4, N_2O, and CFCs [*Ramaswamy et al.*, 1996]. Experiments with full AGCMs yield similar findings [*Wang et al.*, 1991; *Govindasamy et al.*, 2001]. Thus the explicit radiative effects of well-mixed, non-CO_2 greenhouse gases yield less cooling of the lower (and upper) stratosphere than if these trace constituents are treated with an "equivalent CO_2" approximation.

[59] A third but minor factor is our neglect of ECHAM data above 30 hPa (data for the 10 hPa level were not archived). Since stratospheric cooling tends to increase with increasing height in the stratosphere [*Ramaswamy et al.*, 2001], our channel 4 temperature-change estimates neglect a small region of substantial cooling. However, the effect of this omission is almost certainly small due to mass weighting.

[60] In summary, our results suggest that the lower stratospheric temperature-change signal in response to increases in well-mixed greenhouse gases is unlikely to evolve linearly, or show monotonic cooling. The sign of the projected global-mean change in equivalent channel 4 temperatures in the second half of the 21st century may be highly dependent on the specific mix of trace gases employed in the forcing scenario. These signal uncertainties are compounded by uncertainties in the future evolution of stratospheric ozone, which has a large influence on lower stratospheric temperatures [*Ramaswamy et al.*, 1996]. Scenarios of future stratospheric ozone change were not incorporated in any of the ECHAM experiments.

4.4. Tropopause Height Changes in Relation to Vertical Resolution

[61] It is instructive to consider whether the decadal-scale decreases in p_{LRT} in Figure 2 are large relative to the vertical resolution of the AGCMs used to produce these estimates. In the 300-year ECHAM control run, the average pressure of the global-mean annual-mean lapse rate tropopause is at roughly 156 hPa. This was estimated from temperatures archived at discrete pressure levels of 30, 50, 70, 100, 150, 200 hPa, etc. (section 2.2). Thus the vertical resolution of the ECHAM4 AGCM in the vicinity of the global-mean tropopause is roughly 50 hPa (i.e., 200–150 hPa and 150–100 hPa).

[62] Global-mean p_{LRT} values in the ECHAM GHG experiment decrease by roughly 22 hPa over 1860 to 2100 (Figure 8). This overall change is fairly substantial (44%) when measured against the 50 hPa vertical resolution of ECHAM4 in the region of the tropopause. For a standard

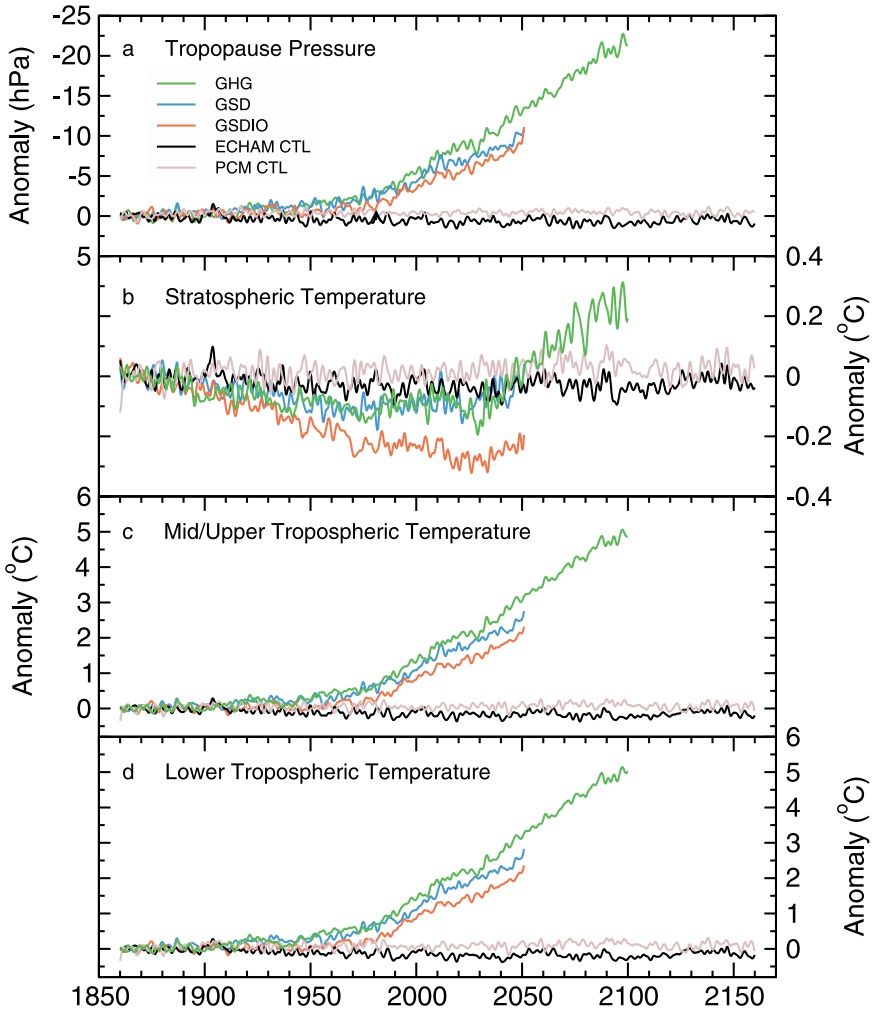

Figure 8. Century-timescale changes in global-mean monthly mean p_{LRT} and layer-average atmospheric temperature. Results are from three climate change experiments and from control runs performed with ECHAM4/OPYC [*Bengtsson et al.*, 1999] and PCM [*Washington et al.*, 2000]. Changes are expressed relative to the smoothed initial state of the experiment (climatological monthly means over 1860–1880). All anomalies are low-pass filtered.

atmosphere, a 22 hPa decrease in the pressure of the tropopause would translate to a tropopause height increase of approximately 950 meters (U.S. Standard Atmosphere, 1976).

[63] In NCEP, global-mean p_{LRT} decreased by 2.16 hPa/decade over 1979 to 2000, corresponding to a linear change in p_{LRT} of −4.8 hPa and a height increase of approximately 200 meters over this 22-year period (section 4.1.1). Like ECHAM4, the assimilation model used by NCEP has vertical resolution of 50 hPa in the region of the global-mean tropopause (section 2.1), so that the overall p_{LRT} change is approximately 10% of the vertical grid spacing at the height of the global-mean tropopause. GISS p_{LRT} changes over 1951–1998 are also roughly 10% of the vertical grid spacing (40 to 50 hPa) at tropopause height.

[64] In all cases considered here, therefore, the decadal- and century-scale global-mean p_{LRT} changes are smaller than the vertical resolution of the model grids at tropopause height. This does not imply that these changes are simply sub-grid-scale noise. The thermal signal that drives the overall p_{LRT} decreases is global in scale, and results in global-scale changes to the static stability of the atmosphere (section 5). Our thermally based algorithm for estimating p_{LRT} is capable of resolving these changes.

[65] The accuracy of our estimated p_{LRT} decreases should be explored further in models with significantly higher vertical resolution than those examined here. We note that the vertical resolution of ECHAM and GISS at the height of the tropopause is similar in the tropics but not in the extratropics (section 2.2). The fact that the overall tropopause height changes in ECHAM and GISS are in close agreement, despite differences in vertical resolution, suggests that our estimates of p_{LRT} changes may be relatively insensitive to any resolution-dependent biases in the estimated time-mean p_{LRT} values.

5. Vertical Profiles of Temperature Change

[66] It is useful to examine the vertical temperature profiles in ECHAM and NCEP in order to understand how p_{LRT} may change in response to external forcing. We first consider annual-mean vertical temperature profiles in

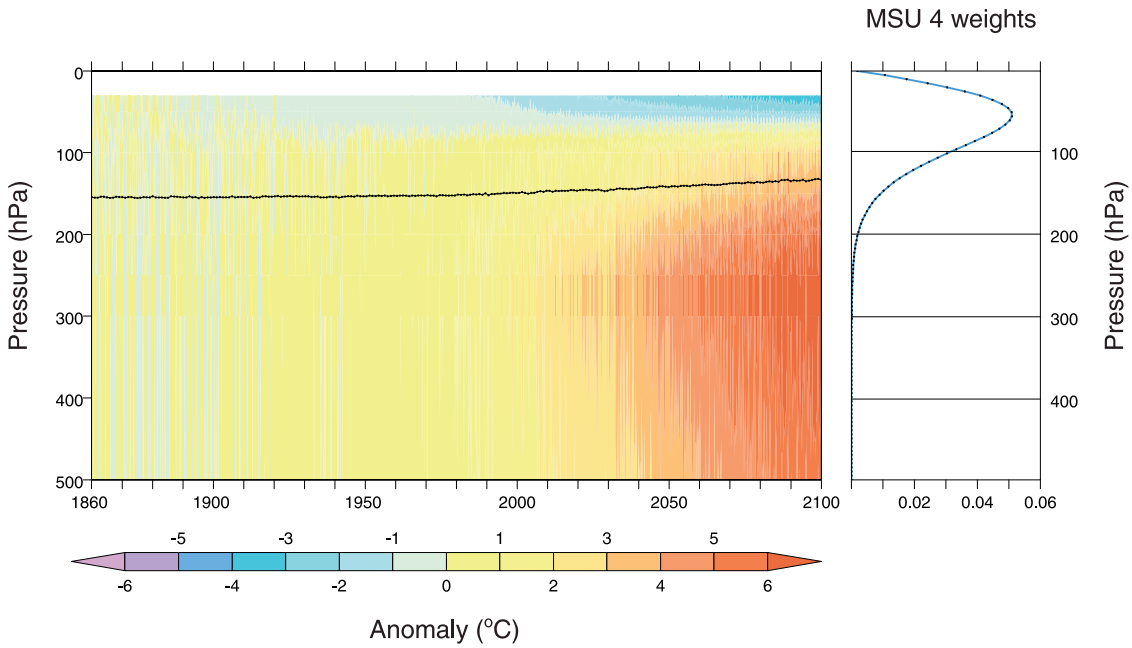

Figure 9. Global-mean monthly mean temperature changes as a function of height in the ECHAM GHG experiment. Changes are defined as in Figure 8. The global-mean weighting function for MSU channel 4 is shown on the right. The vertical scale for the pressure weights is identical to that used for the GHG temperature changes. The black line denotes the estimated global-mean value of p_{LRT} in GHG. See section 4.3 and Figure 12 for further details.

NCEP and GSOP, the ECHAM experiment with forcings most relevant for comparison with observations (Figure 10).

[67] Simulated and observed temperature profiles are very similar at low latitudes. The model cold bias is evident at mid- and high latitudes (above approximately 300 and 400 hPa, respectively [*Gates et al.*, 1999]). The cold bias has no significant effect on the estimated p_{LRT}, except at high latitudes in the Northern Hemisphere.

[68] At low latitudes, the location of the tropopause is well-defined in the time-averaged temperature profiles, and estimated values of p_{LRT} are very close to the transition between large negative and large positive lapse rates (Figure 10). Temperature profiles in mid- to high latitudes have much smaller lapse rates in the vicinity of the tropopause. As a result, p_{LRT} estimates poleward of about 30° are more sensitive to the number of layers used in the interpolation of lapse rates, and the (interpolated) level at which the WMO lapse rate criterion is first satisfied does not necessarily correspond to the level at which lapse rate changes sign (section 2.3).

[69] We next use the ECHAM GHG experiment to consider the effects of well-mixed greenhouse gases on p_{LRT}. This integration is sufficiently long (240 years) to provide a reasonable estimate of the signal in p_{LRT} (Figure 8a).

[70] In general, p_{LRT} changes depend on two factors, both of which have a strong latitudinal dependence: (1) the "baseline" temperature profile $T(z)$ in the control run, particularly at the pressure levels immediately above and below the tropopause; (2) the magnitude and shape of $\Delta T(z)$, i.e., the change in the $T(z)$ profile in response to an external forcing.

[71] To understand how these factors operate, consider an idealized case in which $\Delta T(z)$ increases by 5°C at all model levels below the "baseline" tropopause, is zero above the tropopause, and is latitudinally invariant. The geometry of the control run vertical temperature profiles in Figure 11 dictates that adding these idealized $\Delta T(z)$ values to $T(z)$ would result in a decrease in p_{LRT}, with larger decreases (i.e., a higher tropopause altitude) in the extratropics than in the tropics. This is what actually occurs in both hemispheres in the GHG experiment (Figure 11).

[72] Simulated $\Delta T(z)$ profiles in GHG deviate from this ideal case, and there is large latitudinal variability in the relative temperature changes immediately above and below the tropopause (Figure 12). Three aspects of the $\Delta T(z)$ results are important in interpreting the p_{LRT} changes: (1) Temperature increases immediately below the diagnosed tropopause are largest in the tropics and smallest in the extratropics. Taken alone, this would tend to yield larger p_{LRT} decreases in the tropics than in the extratropics. (2) The warming immediately above the diagnosed tropopause level is also largest in the tropics. This tends to counteract (1): i.e., it would tend to produce smaller p_{LRT} decreases in the tropics than in the extratropics. (3) The net cooling of the stratosphere is larger in the extratropics than in the tropics. This acts in the same direction as item 2 in terms of its effect on p_{LRT}.

[73] These complexities in $\Delta T(z)$ are partly due to the fact that we are dealing with changes in a number of different greenhouse gases. Each of these has different spatio-temporal distributions, radiative properties, and atmospheric temperature responses (see *Govindasamy et al.* [2001] and section 4.3). These differences in $\Delta T(z)$, coupled with latitudinal variations in $T(z)$, make it difficult to determine a priori how a combination of forcings from CO_2 and non-CO_2 greenhouse gases will affect p_{LRT}.

[74] Nevertheless, items 2 and 3 act in the same sense as the latitudinal differences in $T(z)$. All tend to generate larger p_{LRT}

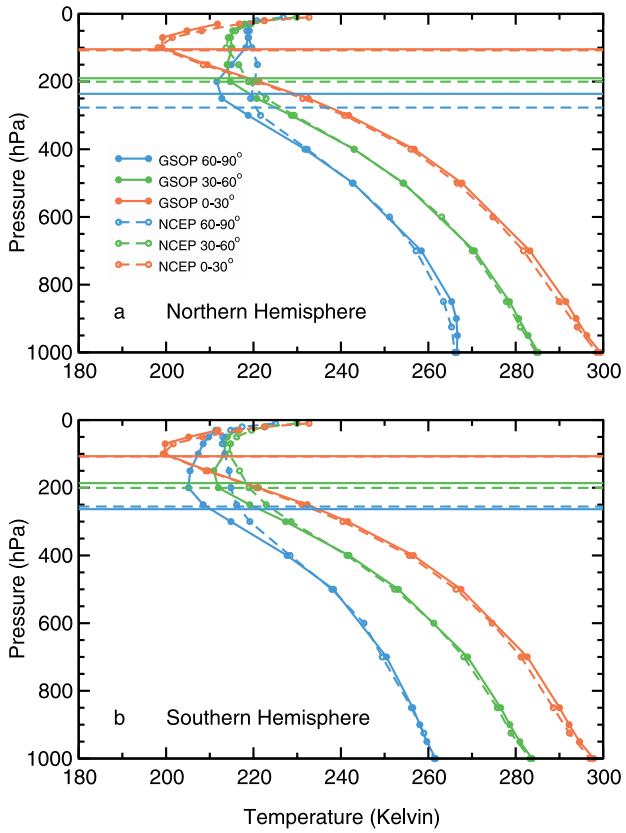

Figure 10. Profiles of annual-mean temperature as a function of height in the NCEP reanalysis and the ECHAM GSOP experiment (section 2). Results are for high-, mid- and low latitudes of the Northern and Southern Hemispheres (panels a and b) and are climatological averages over 1979–1997. The centers of pressure levels are marked. The solid (dashed) horizontal lines give the location of estimated p_{LRT} values in the GSOP (NCEP) data.

decreases in the extratropics than in the tropics. Their net influence apparently outweighs the effect of item 1 above.

[75] We make no attempt here to isolate the effects of volcanoes and stratospheric ozone depletion on vertical temperature profiles, and hence on p_{LRT}. The principal constraint is that the GSO integrations involve simultaneous changes in a number of different forcings (section 2.2). We note, however, that as in the GHG case, ozone-induced cooling of the stratosphere is largest at high latitudes (section 6.2). Stratospheric ozone depletion therefore acts in the same direction as the "baseline geometry" effect, and reinforces the tendency of well-mixed greenhouse gases to cause larger increases in tropopause height in the extratropics.

6. Horizontal Patterns

6.1. Lapse Rate Tropopause

[76] Patterns of annual-mean p_{LRT} changes over 1979 to 1997 are similar in the NCEP reanalysis and the ECHAM climate change experiments (Figure 13). Both have areas of p_{LRT} decrease that are much larger than the areas of p_{LRT} increase. The largest decreases in p_{LRT} are at mid- to high latitudes in both hemispheres, particularly in NCEP and the GSO experiments (see section 5). Areas of increase are found close to the locations of the subtropical jets (at roughly 30°N and 30°S), close to the boundary between the tropical and extratropical tropopause. Since p_{LRT} gradients are very steep at this boundary (Figure 1), relatively small changes in the position or intensity of the jets can lead to large changes in p_{LRT}.

[77] GSDIO, which lacks stratospheric ozone depletion, has smaller p_{LRT} decreases in the extratropics than the three experiments that include this effect. This suggests that the p_{LRT} decrease caused by the larger stratospheric cooling in the GSO integrations outweighs the p_{LRT} decrease caused by the larger tropospheric warming in GSDIO (see Figure 7 and section 4.2).

[78] When the large spatial mean terms are subtracted from the patterns of annual-mean p_{LRT} change, the NCEP and ECHAM spatial anomaly fields are virtually uncorrelated (−0.09 to 0.08; Table 1). There is little indication that increasing realism in the forcing yields greater similarity between the ECHAM and NCEP p_{LRT} changes. We explore this issue in more detail in the paper by Santer et al. (submitted manuscript, 2002).

6.2. Stratospheric Temperature

[79] The simulated changes in stratospheric temperature in the three GSO experiments show strong meridional gra-

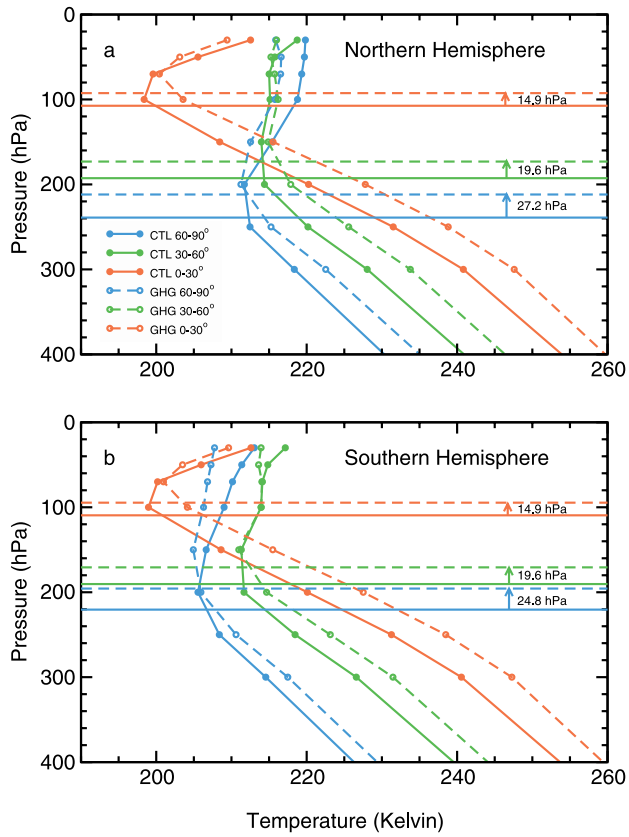

Figure 11. Profiles of annual-mean temperature as a function of height in the ECHAM control run and GHG experiment. Results are climatological averages over 1860–2159 (control) and 2050–2099 (GHG). The change in p_{LRT} between the average control state and the final 50 years of GHG is indicated on the right-hand side of each panel. See Figure 10 and section 5 for further details.

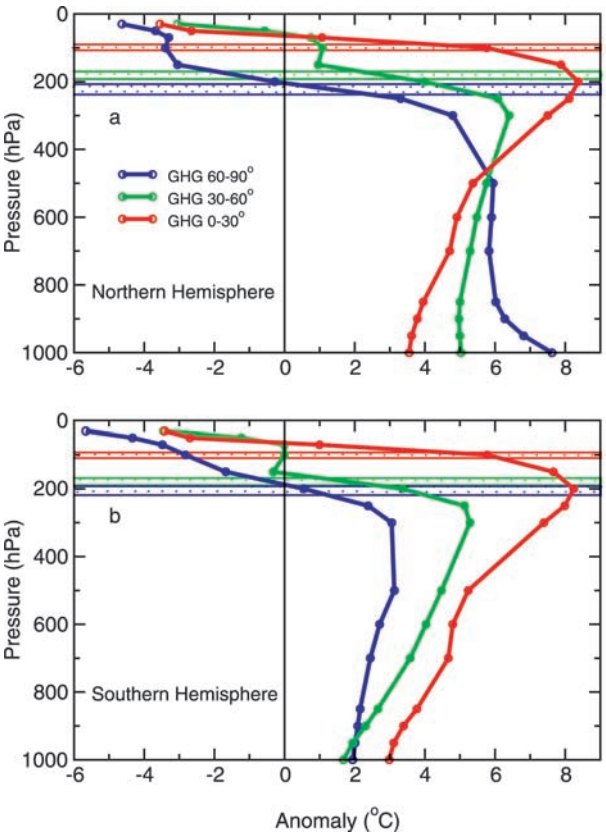

Figure 12. Profiles of changes in annual-mean temperature as a function of height in the ECHAM GHG experiment. Changes are defined as the differences between the smoothed final and initial states of GHG (2079–2099 minus 1860–1880). Climatological-mean p_{LRT} values for 1860–1880 and 2079–2099 are indicated by the lower and upper limits (respectively) of the shaded horizontal bars.

dients, with maximum cooling in polar regions (Figure 14). This is where the largest decreases in stratospheric ozone have occurred over 1979–1997 [*Hansen et al.*, 2002]. Over the Arctic, GSO1 cools by up to 4–5°C more than GSO2, highlighting signal uncertainties arising from internally generated atmospheric variability. GSOP's pattern of change in channel 4 temperature is similar to those of GSO1 and GSO2, since the five-year means that are differenced (1993–1997 minus 1979–1983) largely exclude Pinatubo effects. The cooling resulting from stratospheric ozone depletion is readily apparent by comparing GSDIO results with those of the GSO integrations.

[80] MSU channel 4 data also show the largest cooling in polar regions, but have bands of subsidiary cooling maxima centered at 30°N and 30°S. These bands are absent in the GSO integrations, but do appear in the NCEP data. The global-mean cooling is considerably larger in NCEP and MSUd than in the GSO integrations (Figure 7b). Unlike the p_{LRT} results, increasing realism of the forcing does translate to greater similarity between modeled and observed global-mean changes.

[81] The NCEP and MSU patterns of stratospheric temperature change are very similar poleward of 60°, but NCEP's cooling substantially exceeds that of MSU between roughly 45°N–45°S (Figures 14e and 14f). Possible explanations for these differences were discussed in section 4.1.2.

[82] The pattern correlation results confirm that stratospheric temperature changes in GSDIO are dissimilar to the changes in either NCEP or MSUd (Table 1). Spatial anomaly correlations are consistently negative for NCEP/GSO comparisons and positive for MSUd/GSO comparisons. Most of this sensitivity to the choice of observed data set probably arises from the excessive cooling of NCEP's stratospheric temperatures in the tropics. In comparisons between GSO and MSUd, greater realism in the forcing enhances the similarity between simulated and observed temperature-change patterns.

6.3. Midtropospheric to Upper Tropospheric Temperature

[83] Simulated temperature changes in the mid- to upper troposphere (Figure 15) also show a clear signal in response to the imposed stratospheric ozone depletion in the GSO integrations. Equivalent channel 2 temperatures in GSO1, GSO2, and GSOP cool by up to −0.6 to −0.8°C over the Arctic and Antarctic. This polar cooling is absent in the GSDIO integration without ozone depletion, but is present in actual MSU channel 2 data.

[84] The most prominent differences between mid- to upper-tropospheric temperatures in the GSO experiments and MSU are between ca. 30°N–30°S, where the simulations warm and MSU cools. NCEP's cooling over the same region is 0.2 to 0.4°C larger than in MSU. This is reflected in the large differences in global-mean channel 2 trends in NCEP and MSU (see Figure 7c and section 4.1.3). In common with results for stratospheric temperatures, GSO spatial anomalies are more similar to MSUd than to NCEP (Table 1 and section 6.2). A further commonality is that the pattern of mid- to upper-tropospheric temperature change in MSUd is more highly correlated with the GSO anomaly fields (with more realistic forcing) than with the GSDIO pattern.

6.4. Lower Tropospheric Temperature

[85] Lower tropospheric temperature changes (Figure 16) are spatially noisier than the temperature changes in channels 2 and 4. As for channel 2, MSU and NCEP 2LT data cool in the tropics and subtropics, while all four model simulations warm. The simulated and observed patterns of 2LT change are virtually uncorrelated (Table 1). The MSU and NCEP temperature-change patterns are more similar for the 2LT retrieval than for channels 4 and 2.

[86] There is a tendency toward larger lower tropospheric temperature increases at the poles and a net decrease in the equator-to-pole temperature gradient. Exceptions are GSOP in the Northern Hemisphere and MSUd in the Southern Hemisphere. *Held* [1982] has suggested that an increase in equator-to-pole temperature gradient might increase baroclinicity and raise the height of the extratropical tropopause. In the model experiments of *Thuburn and Craig* [1997], the opposite result occurred: increasing (decreasing) the equator-to-pole temperature gradient lowered (raised) tropopause height in the extratropics.

[87] The findings of *Thuburn and Craig* [1997] help to explain two aspects of our results. The first aspect is the previously noted tendency toward larger changes in p_{LRT} at

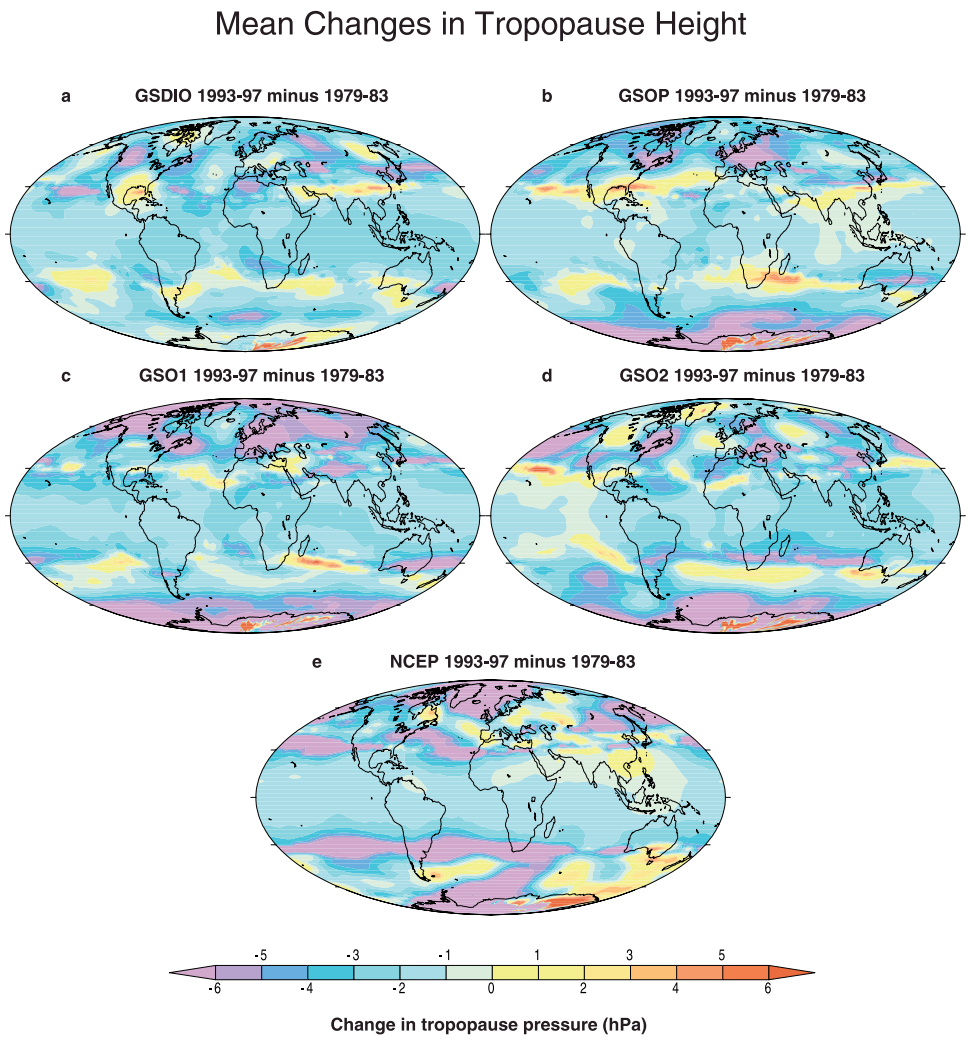

Figure 13. Changes in annual-mean p_{LRT} patterns in four ECHAM climate change experiments (panels a–d) and in the NCEP reanalysis (panel e). Changes are defined as the average over 1993–1997 minus the average over 1979–1983.

mid- to high latitudes in both hemispheres, a feature common to the NCEP and ECHAM results (Figures 11 and 13). This pattern of p_{LRT} change may be due not only to the pronounced latitudinal dependence of $T(z)$ and $\Delta T(z)$ in the vicinity of the tropopause (section 5), but also to the larger high-latitude surface warming in response to increased greenhouse gases, and the attendant reduction in equator-to-pole temperature gradient.

[88] The second aspect of our results that is clarified is the increase in tropopause height in the NCEP reanalysis over 1979–1997, despite the overall cooling of NCEP's troposphere during this period (Figures 7c and 7d). Some of this increase is attributable to excessive stratospheric cooling in NCEP (Figure 7b and section 4.1.2). The *Thuburn and Craig* [1997] results suggest that NCEP's tropopause height increase is also due to a reduction in the equator-to-pole temperature gradient, a feature common to NCEP and the ECHAM simulations (Figure 16).

6.5. Temperature Influences on Patterns of Tropopause Height Change

[89] The results in sections 4.2 and 6.1–6.4 suggest that decadal-timescale changes in p_{LRT} are influenced by temperature variability in both the troposphere and lower stratosphere. Here, we use pattern correlations to quantify these relationships.

[90] Large meridional gradients in the patterns of changes in p_{LRT} and layer-averaged temperature (Figures 13 and 14–16, respectively) make it difficult to evaluate pattern corre-

Table 1. Pattern Correlations Between Simulated Annual-Mean Changes in p_{LRT} and Atmospheric Temperature and Corresponding Changes in the NCEP Reanalysis and MSUd[a]

	GSDIO	GSO1	GSO2	GSOP
NCEP p_{LRT}	−0.09	0.05	0.08	0.05
NCEP Channel 4	0.13	−0.39	−0.32	−0.38
NCEP Channel 2	0.00	−0.04	−0.03	−0.08
NCEP 2LT	−0.01	0.00	0.02	−0.12
MSUd Channel 4	0.16	0.28	0.28	0.32
MSUd Channel 2	0.08	0.30	0.26	0.22
MSUd 2LT	−0.08	0.07	0.09	−0.19

[a]Changes are defined as the mean over 1993–1997 minus the mean over 1979–1983. Model results were interpolated to the resolution of the NCEP or MSUd data. The spatial means of the two fields being compared were subtracted. For full information on data sources, refer to section 2. Note that p_{LRT} could not be computed from MSUd data.

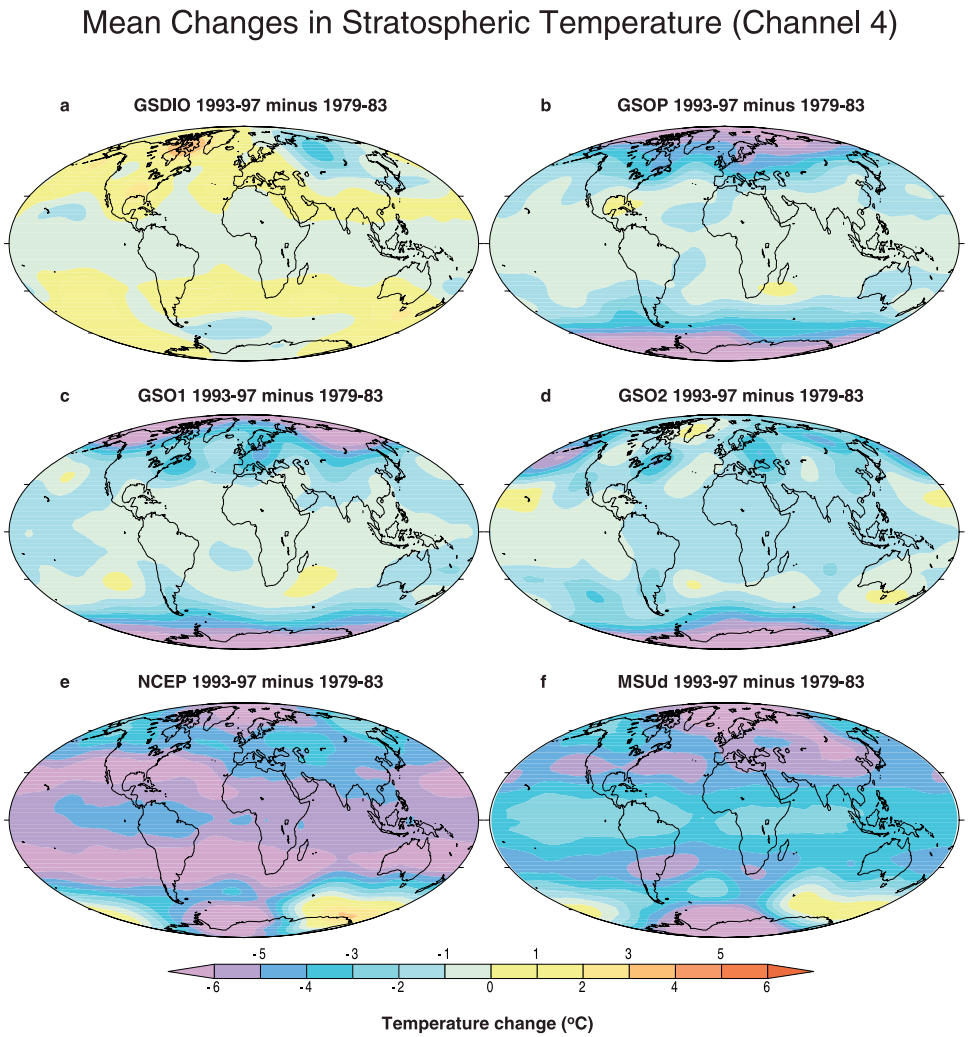

Figure 14. Changes in annual-mean stratospheric temperature in four ECHAM climate change experiments (panels a–d), the NCEP reanalysis (panel e), and actual MSU channel 4 data (panel f). See Figure 13 for definition of changes.

spondence on regional scales. We therefore computed two forms of pattern correlation, the first subtracting the overall spatial means of the two fields being compared, and the second subtracting the respective zonal means. We refer to these below as r_{GLOBAL} and r_{ZONAL}.

[91] The largest r_{GLOBAL} values are between changes in lower stratospheric temperature and p_{LRT} in the GSO1, GSO2, and GSOP experiments with stratospheric ozone depletion (r_{GLOBAL} = 0.60, 0.52, and 0.51, respectively; see Table 2). These high values are primarily due to the pronounced meridional gradients in p_{LRT} and channel 4 temperatures. GSDIO lacks ozone depletion and has weaker meridional gradients, leading to a lower correlation (r_{GLOBAL} = 0.41). The global correlation between changes in p_{LRT} and lower stratospheric temperature is weakest for NCEP (r_{GLOBAL} = 0.36).

[92] Patterns of decadal-timescale p_{LRT} changes are more highly anticorrelated with changes in the 2LT retrieval than with changes in channel 2 temperatures. The largest absolute r_{GLOBAL} values are for GSDIO (r_{GLOBAL} = −0.50 for p_{LRT} versus 2LT), which has the largest tropospheric warming in the four ECHAM integrations.

[93] In the GSO experiments, correlations between p_{LRT} and channel 4 anomaly patterns have r_{ZONAL} values that are considerably smaller than r_{GLOBAL} (Table 2). This indicates that the pattern similarity is primarily dictated by the strong equator-to-pole gradient in both the p_{LRT} changes and the channel 4 temperature response to stratospheric ozone depletion. In contrast, r_{GLOBAL} and r_{ZONAL} values are quite similar for correlations between p_{LRT} and 2LT changes. In this case, the large r_{GLOBAL} value for GSDIO (Table 2) does not arise through meridional gradients alone. Absolute values of r_{ZONAL} in NCEP are always larger than r_{GLOBAL}.

[94] These results support our finding that the global-scale features of the ECHAM p_{LRT} changes are an integrated response to both the warming of the troposphere and the cooling of the stratosphere (section 4.2).

7. Summary and Conclusions

[95] The premise underlying this work is that anthropogenically forced climate change should be evident in many aspects of the climate system, and not simply in "traditional" detection variables, such as temperatures at the

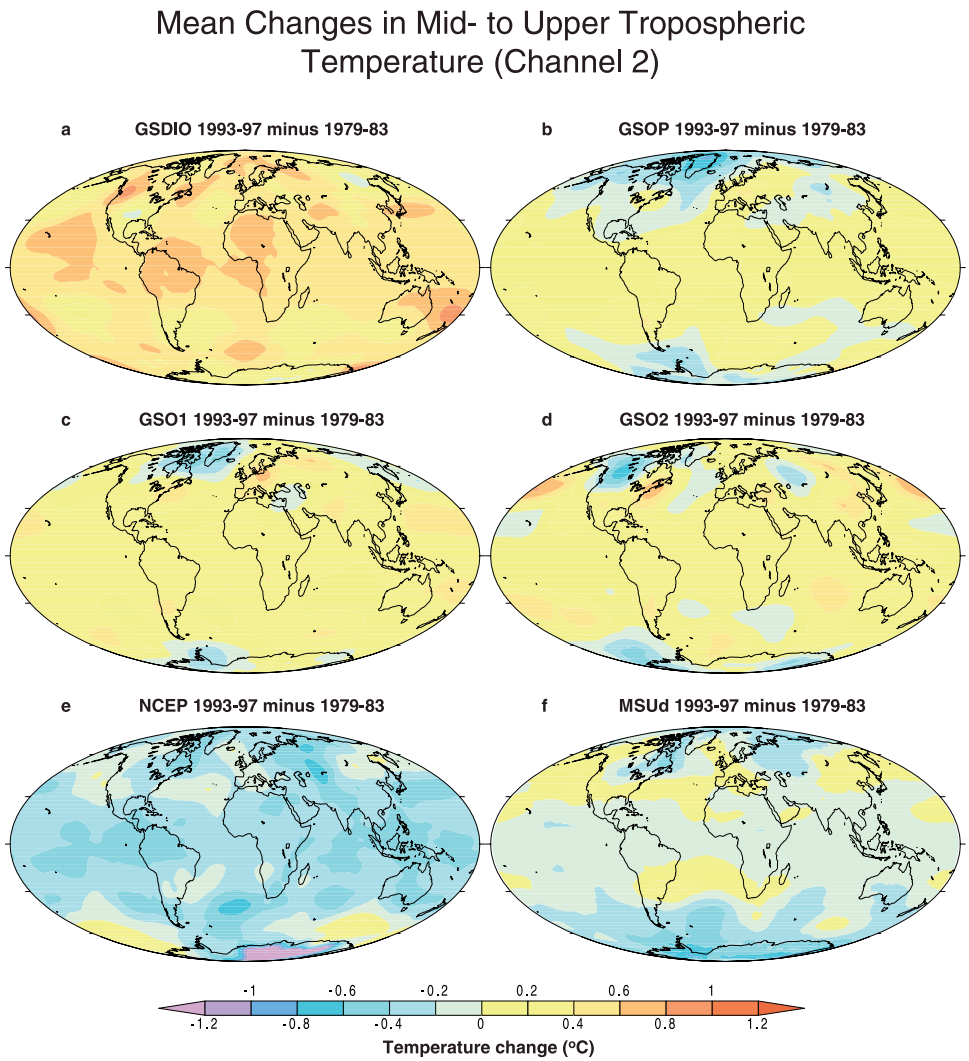

Figure 15. As for Figure 13, but for changes in annual-mean mid- to upper-tropospheric temperature.

Earth's surface or in the free atmosphere. To test this premise, we introduce a diagnostic that has not been used in previous detection studies: changes in p_{LRT}, the pressure of the lapse rate tropopause.

[96] We estimated p_{LRT} values from two different reanalysis products (NCEP and ERA) and from climate change experiments performed with two different models (ECHAM and GISS). All had relatively coarse vertical resolution in the atmosphere, ranging from 12 to 19 discrete pressure levels. To diagnose p_{LRT}, we applied the same WMO-based algorithm to the model and reanalysis vertical temperature data.

[97] We find pronounced increases in tropopause height (corresponding to a decrease in p_{LRT}) in both the reanalysis and model datasets (Figure 2). In the NCEP reanalysis, global-mean p_{LRT} decreased by 2.16 hPa/decade over 1979–2000, with the largest decreases occurring in the extratropics. The shorter ERA reanalysis has a global-mean p_{LRT} trend of −1.13 hPa/decade over 1979–1993. The decreases in tropical p_{LRT} that we derived from the reanalyses are consistent with those estimated from radiosondes [*Seidel et al.*, 2001]. They are also in accord with recent evidence for an intensification of the Hadley circulation over the past decade [*Chen et al.*, 2002]. Superimposed on these overall declines in p_{LRT} are pronounced increases in tropopause pressure in response to the eruptions of El Chichón in 1982 and Pinatubo in 1991 (Figure 2).

[98] Many aspects of this behavior are reproduced in the ECHAM GSOP experiment [*Roeckner et al.*, 1999; *Bengtsson et al.*, 1999] and in the GISS SI2000 integrations [*Hansen et al.*, 2002]. The former employs a coupled atmosphere-ocean GCM forced by changes well-mixed greenhouse gases, direct and indirect sulfate aerosol effects, stratospheric and tropospheric ozone, and stratospheric aerosols from the Pinatubo eruption. We also consider results from ECHAM experiments that exclude certain of the GSOP forcings.

[99] The GISS climate change experiment was performed with an atmospheric GCM driven by observed time-varying SSTs and sea-ice coverage, as well as by changes in six different external forcings (section 2.2). Five realizations of the GISS experiment were available, each with the same forcing but commencing from different atmospheric initial conditions.

[100] The global-mean p_{LRT} trends over 1979–1997 are negative in both GSOP (−1.47 hPa/decade) and in the five-member GISS ensemble (from −1.30 to −1.52 hPa/dec-

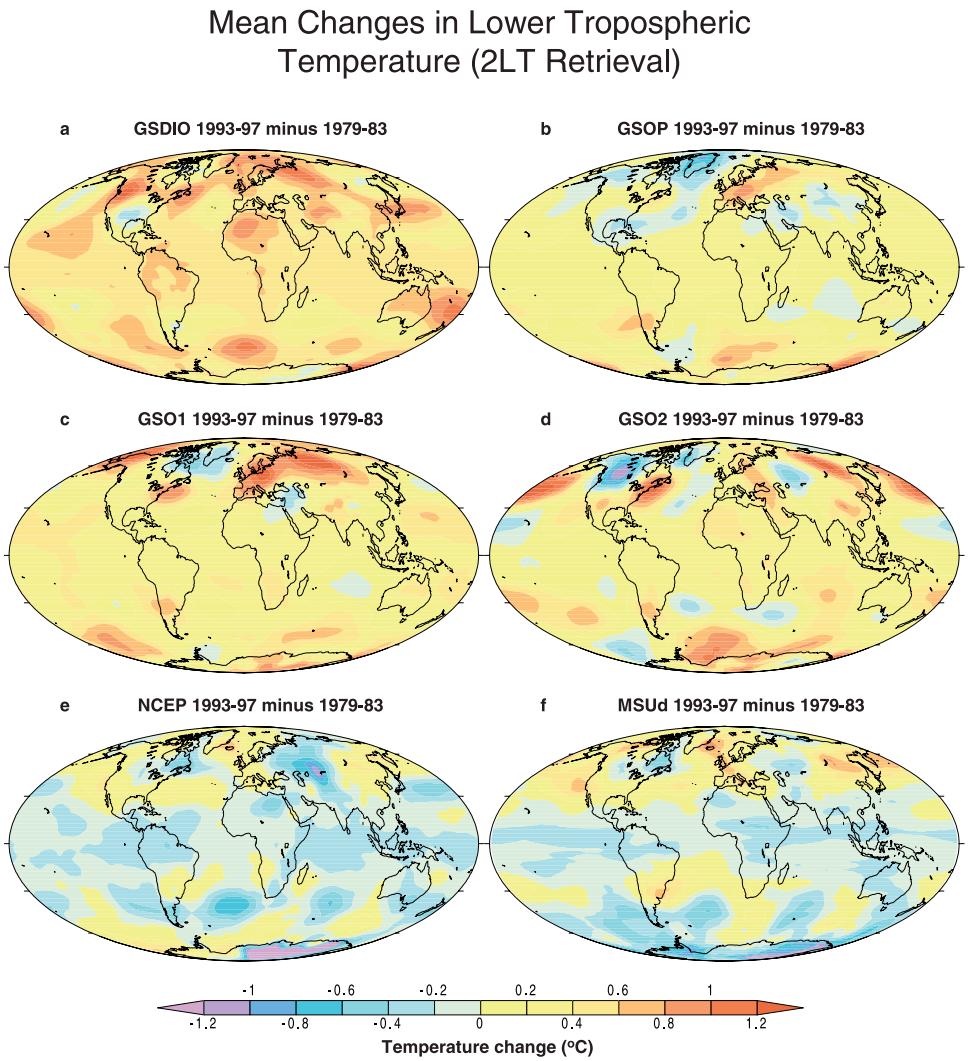

Figure 16. As for Figure 13, but for changes in annual-mean lower-tropospheric temperature.

ade). These values are smaller than (but not significantly different from) NCEP's p_{LRT} trend of −1.82 hPa/decade over the same period. In addition to this low-frequency agreement between models and reanalyses, there is also agreement in the response to volcanic forcing: p_{LRT} increases after Pinatubo (i.e., tropopause height decreases). However, the amplitude of the p_{LRT} response to Pinatubo is larger in both ECHAM and GISS simulations than in either reanalysis (Figure 2).

[101] Possible explanations for these results are provided by our analysis of vertical temperature profiles. For highly idealized profiles of temperature change, simple geometrical considerations dictate that tropopause height should do the following: (1) increase in response to warming of the troposphere and cooling of the stratosphere caused by increases in well-mixed greenhouse gases; (2) increase due to cooling of the stratosphere induced by stratospheric ozone depletion; (3) decrease after the stratospheric warming and tropospheric cooling resulting from massive volcanic eruptions.

[102] Such simplified interpretations of p_{LRT} changes are complicated by two factors. The first is the initial or "baseline" temperature profile, $T(z)$. The second is the magnitude and shape of $\Delta T(z)$, the change in $T(z)$ in response to a specified external forcing. Both $T(z)$ and $\Delta T(z)$ depend strongly on latitude. Furthermore, $\Delta T(z)$ may be very different from the idealized changes described

Table 2. Pattern Correlations Between Annual-Mean Changes in Layer-Averaged Atmospheric Temperature and p_{LRT}[a]

Comparison	GSDIO	GSO1	GSO2	GSOP	NCEP
p_{LRT} vs. Channel 4	0.41 (0.40)	0.60 (0.31)	0.52 (0.39)	0.51 (0.28)	0.36 (0.52)
p_{LRT} vs. Channel 2	−0.45 (−0.47)	0.11 (−0.29)	−0.20 (−0.38)	0.12 (−0.21)	0.05 (−0.08)
p_{LRT} vs. 2LT	−0.50 (−0.49)	−0.38 (−0.30)	−0.40 (−0.36)	−0.27 (−0.21)	−0.19 (−0.27)

[a]Changes are defined as in Table 1. The overall spatial means of the patterns being compared are subtracted; numbers in brackets are anomaly correlations after subtraction of zonal means.

above. For example, forcing by well-mixed greenhouse gases in the ECHAM GHG experiment eventually leads to warming of the lower stratosphere (between approximately 70–150 hPa for global-mean data; see Figure 8 and section 4.3) rather than cooling.

[103] Despite these complexities in $T(z)$ and $\Delta T(z)$, the global-mean p_{LRT} behavior that we observe in the ECHAM and GISS model simulations is in reasonable accord with expectations based on idealized temperature-change profiles. There is also some correspondence between the simulated and observed large-scale patterns of p_{LRT} change over 1979–1997. In both reanalyses and the ECHAM simulations, the largest overall decreases in p_{LRT} are in the extratropics (Figure 13). (Detailed patterns of p_{LRT} change were not analyzed for the GISS experiment.)

[104] The latter result arises from the strong latitudinal dependence of $T(z)$ and $\Delta T(z)$. Latitudinal differences in the initial $T(z)$ profiles should, on geometric grounds alone, yield larger p_{LRT} changes in the extratropics than in the tropics, even for latitudinally uniform $\Delta T(z)$ (Figure 11). However, $\Delta T(z)$ is not uniform with latitude or height. For stratospheric cooling induced by ozone (Figure 14) and well-mixed greenhouse gases (Figure 12), $\Delta T(z)$ tends to be amplified toward the poles. In the well-mixed greenhouse gas case, the warming immediately above the tropopause is larger in the tropics than the extratropics. These factors reinforce the "initial $T(z)$ geometry" effect: all lead to larger p_{LRT} changes in the extratropics (section 5).

[105] Taken together, our results provide a plausible explanation of the high-latitude amplification of p_{LRT} decreases in NCEP and the ECHAM GSOP, GSO1, and GSO2 experiments (which we collectively refer to as "GSO"). They also shed light on a puzzling question: Why do NCEP and the GSO integrations have similar global-mean p_{LRT} trends, despite very different trends in tropospheric temperature?

[106] Some of this similarity is fortuitous, and is likely related to an error in NCEP's lower stratospheric temperatures. The cooling of the lower stratosphere in NCEP is significantly larger than in the *Christy et al.* [2000] MSU data (Figure 7b), probably due to biases in both the radiosonde data [*Lanzante et al.*, 2002] and the NESDIS temperature retrievals assimilated by NCEP [*Santer et al.*, 1999]. Taken alone, this would lead to an excessive decrease in p_{LRT} in NCEP. This decrease is apparently offset by NCEP's spuriously large tropospheric cooling (relative to MSU data; Figure 7).

[107] Recent investigations of tropospheric temperature data by *Wentz et al.* [2001] and Lanzante et al. (submitted manuscript, 2002) highlight the large uncertainties in current satellite- and radiosonde-based estimates of tropospheric temperature change. These two studies suggest that tropospheric temperature changes over the satellite era may have been underestimated. If the Wentz et al. and Lanzante et al. results are correct, p_{LRT} changes in the real world and in model simulations would be occurring for similar reasons: the combined effect of warming of the troposphere and cooling of the lower stratosphere. This underscores the importance of reducing uncertainties in satellite- and radiosonde-based estimates of atmospheric temperature change.

[108] The NCEP results illustrate that tropopause height changes should not be examined in isolation, without knowledge of the stratospheric and tropospheric temperature changes that drive variations in p_{LRT}. They also imply that detection studies based on global-mean p_{LRT} changes may yield misleading results. In a companion paper (Santer et al., submitted manuscript, 2002), our detection strategy is based on the latitude/longitude patterns of temperature and p_{LRT} changes rather than on global-mean values. Use of spatial pattern information makes it more difficult to obtain significant but spurious model/data similarities. Santer et al. (submitted manuscript, 2002) show that the model-predicted pattern of p_{LRT} change in response to anthropogenic forcing is detectable in both the ERA and NCEP reanalyses. In the latter case, this partly reflects our present finding that some component of the NCEP/GSO similarity in p_{LRT} changes is real and related to their common pattern of high-latitude amplification of lower stratospheric cooling and lower tropospheric warming (section 5).

[109] The ECHAM results in Figure 7 indicate that both stratospheric ozone depletion and increases in well-mixed GHGs contribute to the overall increases in tropopause height. It would be useful to estimate the relative contributions of both factors to the simulated p_{LRT} changes over the satellite era. Obtaining reliable estimates of these contributions will require multiple realizations of experiments in which well-mixed GHGs and stratospheric ozone are varied individually rather than jointly. Such ensembles were not available for this study.

[110] The pronounced increases in tropopause height in both the ECHAM and GISS climate change integrations contradict suggestions that AGCMs with relatively coarse vertical resolution may be incapable of resolving small externally forced changes in tropopause height [*Ramaswamy et al.*, 2001]. We find that the simulated decadal-scale changes in p_{LRT} are primarily thermally driven and are an integrated measure of the anthropogenically forced warming of the troposphere and cooling of the stratosphere. Our algorithm for estimating p_{LRT} (based on a thermal definition of the tropopause) is sufficiently sensitive to resolve these large-scale changes in atmospheric thermal structure. Further experimentation is necessary to determine the sensitivity of both changes in p_{LRT} and climatological-mean p_{LRT} values to substantial increases in vertical resolution.

[111] In summary, our results indicate that the simulated increase in tropopause height over 1979–1997 is a robust, zero-order response of the climate system to forcing by well-mixed greenhouse gases and stratospheric ozone depletion. At the global-mean level, we find agreement between the simulated decadal-scale p_{LRT} changes and those estimated from reanalyes. While this agreement is partly fortuitous, it is also driven by real pattern similarities. Our work illustrates that changes in tropopause height may be a useful "fingerprint" of human effects on climate and are deserving of further attention.

Appendix A: Use of Monthly Mean Data for Calculation of Tropopause Pressure

[112] Since the procedure for estimating p_{LRT} is nonlinear, it is important to check that the temporal resolution of the input temperature data does not bias the results. To verify this, we used NCEP's own six-hourly estimates of p_{LRT} (computed on model hybrid coordinates rather than pressure levels), and then averaged these to form monthly

mean p_{LRT} values. These results were then compared with our own independently derived p_{LRT} estimates based on monthly mean temperature data from NCEP (section 2.3).

[113] The two sets of global-mean monthly mean p_{LRT} anomalies are highly correlated ($r = 0.96$) and have similar least-squares linear trends over 1979–2000 (−1.84 hPa/decade for 6-hourly and −2.16 hpa/decade for monthly mean NCEP data; see Figure 2a). The slight differences probably arise through differences in both the algorithms used to compute p_{LRT} and in the criteria employed to identify high-latitude grid-points where p_{LRT} may be undefined at certain times of year [*Reichler et al.*, 1996]. The latter effect would explain why the two sets of NCEP p_{LRT} results are more similar in the tropics ($r = 0.98$; Figure 2a) than in the globally averaged data.

[114] This close agreement between p_{LRT} values based on 6-hourly and monthly mean temperatures justifies our uses of monthly mean temperature data for calculating p_{LRT}.

[115] **Acknowledgments.** This work was initiated during a stimulating sabbatical (sponsored by "Freunde des DLR") that Robert Sausen spent at PCMDI. Work at Lawrence Livermore National Laboratory was performed under the auspices of the U.S. Department of Energy, Environmental Sciences Division, under contract W-7405-ENG-48. Tom Wigley received support from the NOAA Office of Global Programs ("Climate Change Data and Detection") under grant NA87GP0105. Jerry Meehl was supported by the Office of Biological and Environmental Research, U.S. Department of Energy, as part of its Climate Change Prediction Program. The authors would like to acknowledge the assistance of Mike Wehner (PCMDI) and Monika Esch (Max-Planck Institute for Meteorology) in the transfer and processing of model data. Results from the ECHAM4/OPYC simulations were kindly provided by Lennart Bengtsson (MPI). John Lanzante, V. Ramaswamy and Ron Stouffer (all GFDL), Mike MacCracken (U.S. Global Change Research Program) and Kevin Trenberth (NCAR) provided useful comments and suggestions.

References

Allen, M. R., et al., Quantifying anthropogenic influence on recent near-surface temperature change, *Surv. Geophys.*, in press, 2002.

Andronova, N. G., E. V. Rozanov, F. Yang, and M. E. Schlesinger, Radiative forcing by volcanic aerosols from 1850 to 1994, *J. Geophys. Res.*, *104*, 16,807–16,826, 1999.

Barnett, T. P., D. W. Pierce, and R. Schnur, Detection of anthropogenic climate change in the world's ocean, *Science*, *292*, 270–274, 2001.

Basist, A. N., and M. Chelliah, Comparison of tropospheric temperatures derived from the NCEP/NCAR reananlysis, NCEP operational analysis, and the Microwave Sounding Unit, *Bull. Am. Meteorol. Soc.*, *7*, 1431–1447, 1997.

Bengtsson, L., E. Roeckner, and M. Stendel, Why is the global warming proceeding much slower than expected?, *J. Geophys. Res.*, *104*, 3865–3876, 1999.

Boville, B. A., and J. W. Hurrell, A comparison of the atmospheric circulations simulated by CCM3 and CSM1, *J. Clim.*, *11*, 1327–1341, 1998.

Chen, J., B. E. Carlson, and A. D. Del Genio, Evidence for strengthening of the tropical general circulation in the 1990s, *Science*, *295*, 838–841, 2002.

Christy, J. R., R. W. Spencer, and W. D. Braswell, MSU tropospheric temperatures: Dataset construction and radiosonde comparisons, *J. Atmos. Oceanic Technol.*, *17*, 1153–1170, 2000.

Dameris, M., D. Nodorp, and R. Sausen, Correlation between tropopause height pressure and TOMS data for the EASOE-winter 1991/1992, *Contrib. Atmos. Phys.*, *68*, 227–232, 1995.

Forster, P., R. S. Freckleton, and K. P. Shine, On aspects of the concept of radiative forcing, *Clim. Dyn.*, *13*, 547–560, 1997.

Gates, W. L., et al., An overview of the results of the Atmospheric Model Intercomparison Project (AMIP I), *Bull. Am. Meteorol. Soc.*, *80*, 29–55, 1999.

Gibson, J. K., P. Kållberg, S. Uppala, A. Hernandez, A. Nomura, and E. Serrano, ERA description, *ECMWF Re-anal. Proj. Rep. Ser. 1*, 66 pp., Eur. Cent. for Medium-Range Weather Forecasts, Reading, England, 1997.

Govindasamy, B., K. E. Taylor, P. B. Duffy, B. D. Santer, A. S. Grossman, and K. E. Grant, Limitations of the equivalent CO_2 approximation in climate change simulations, *J. Geophys. Res.*, *106*, 22,593–22,603, 2001.

Hansen, J. E., et al., Forcing and chaos in interannual to decadal climate change, *J. Geophys. Res.*, *102*, 25,679–25,720, 1997.

Hansen, J. E., M. Sato, J. Glascoe, and R. Ruedy, A common-sense climate index: Is climate changing noticeably?, *Proc. Natl. Acad. Sci. U. S. A.*, *95*, 4113–4120, 1998.

Hansen, J. E., et al., Climate forcings in Goddard Institute for Space Studies SI2000 simulations, *J. Geophys. Res*, *107*(D18), 4347, doi:10.1029/2001JD001143, 2002.

Haynes, P., J. Scinocca, and M. Greenslade, Formation and maintenance of the extratropical tropopause by baroclinic eddies, *Geophys. Res. Lett.*, *28*, 4179–4182, 2001.

Hegerl, G. C., H. von Storch, K. Hasselmann, B. D. Santer, U. Cubasch, and P. D. Jones, Detecting greenhouse-gas-induced climate change with an optimal fingerprint method, *J. Clim.*, *9*, 2281–2306, 1996.

Hegerl, G. C., K. Hasselmann, U. Cubasch, J. F. B. Mitchell, E. Roeckner, R. Voss, and J. Waszkewitz, Multi-fingerprint detection and attribution analysis of greenhouse gas, greenhouse gas-plus-aerosol and solar forced climate change, *Clim. Dyn.*, *13*, 613–634, 1997.

Held, I. M., On the height of the tropopause and the static stability of the atmosphere, *J. Atmos. Sci.*, *39*, 412–417, 1982.

Hoinka, K. P., Statistics of the global tropopause pressure, *Mon. Weather Rev.*, *126*, 3303–3325, 1998.

Houghton, J. T., L. G. Meira Filho, B. A. Callander, N. Harris, A. Kattenberg, and K. Maskell, *Climate Change 1995: The Science of Climate Change*, 572 pp., Cambridge Univ. Press, New York, 1996.

Houghton, J. T., Y. Ding, D. J. Griggs, M. Noguer, P. J. van der Linden, X. Dai, K. Maskell, and C. A. Johnson, *Climate Change 2001: The Scientific Basis*, 881 pp., Cambridge Univ. Press, New York, 2001.

Kalnay, E., et al., The NCEP/NCAR 40-year reanalysis project, *Bull. Am. Meteorol. Soc.*, *77*, 437–471, 1996.

Karl, T. R., R. W. Knight, D. R. Easterling, and R. G. Quayle, Indices of climate change for the United States, *Bull. Am. Meteorol. Soc.*, *77*, 279–292, 1996.

Karoly, D. J., and K. Braganza, Identifying global climate change using simple indices, *Geophys. Res. Lett.*, *28*, 2205–2208, 2001.

Karoly, D. J., J. A. Cohen, G. A. Meehl, J. F. B. Mitchell, A. H. Oort, R. J. Stouffer, and R. T. Wetherald, An example of fingerprint detection of greenhouse climate change, *Clim. Dyn.*, *10*, 97–105, 1994.

Kirchner, I., G. L. Stenchikov, H.-F. Graf, A. Robock, and J. C. Antuña, Climate model simulation of winter warming and summer cooling following the 1991 Mount Pinatubo volcanic eruption, *J. Geophys. Res.*, *104*, 9039–9055, 1999.

Lanzante, J. R., et al., Temporal homogenization of monthly radiosonde temperature data, part II, Trends, sensitivities, and MSU comparison, *J. Clim.*, in press, 2002.

Meehl, G. A., P. Gent, J. M. Arblaster, B. Otto-Bliesner, E. Brady, and A. Craig, Factors that affect amplitude of El Niño in global coupled climate models, *Clim. Dyn.*, *17*, 515–526, 2000.

Mitchell, J. F. B., D. J. Karoly, G. C. Hegerl, F. W. Zwiers, M. R. Allen, and J. Marengo, Detection of climate change and attribution of causes, in *Climate Change 2001: The Scientific Basis*, edited by J. T. Houghton et al., pp. 695–738, Cambridge Univ. Press, New York, 2001.

Mo, K., X. L. Wang, R. Kistler, M. Kanamitsu, and E. Kalnay, Impact of satellite data on the CDAS-reanalysis system, *Mon. Weather Rev.*, *123*, 124–139, 1995.

Oberhuber, J. M., Simulation of the Atlantic circulation with a coupled sea-ice mixed-layer isopycnal general circulation model I, Model description, *J. Phys. Oceanogr.*, *22*, 808–829, 1993.

Pawson, S., and M. Fiorino, A comparison of reanalyses in the tropical stratosphere, Part 1, Thermal structure and the annual cycle, *Clim. Dyn.*, *14*, 631–644, 1998.

Press, W. H., B. P. Flannery, S. A. Teukolsky, and W. T. Vetterling, *Numerical Recipes: The Art of Scientific Computing*, 818 pp., Cambridge Univ. Press, New York, 1986.

Ramaswamy, V., M. D. Schwarzkopf, and W. J. Randel, Fingerprint of ozone depletion in the spatial and temporal pattern of recent lower-stratospheric cooling, *Nature*, *382*, 616–618, 1996.

Ramaswamy, V., et al., Stratospheric temperature trends: Observations and model simulations, *Rev. Geophys.*, *39*, 71–122, 2001.

Randel, W. J., F. Wu, and D. J. Gaffen, Interannual variability of the tropical tropopause derived from radiosonde data and NCEP reanalyses, *J. Geophys. Res.*, *105*, 15,509–15,523, 2000.

Reichler, T., M. Dameris, R. Sausen, and D. Nodorp, A global climatology of the tropopause height based on ECMWF analyses, *Inst. für Phys. der Atmos. Rep. 57*, 23 pp., Dtsch. Forschungsanst. für Luft und Raumfahrt, Wessling, Germany, 1996.

Reid, G. C., and K. S. Gage, On the annual variation in height of the tropical tropopause, *J. Atmos. Sci.*, *38*, 1928–1938, 1981.

Reid, G. C., and K. S. Gage, A relationship between the height of the tropical tropopause and the global angular momentum of the atmosphere, *Geophys. Res. Lett.*, *1*, 840–842, 1984.

Reid, G. C., and K. S. Gage, Interannual variations in the height of the tropical tropopause, *J. Geophys. Res.*, *90*, 5629–5635, 1985.

Roeckner, E., J. M. Oberhuber, A. Bacher, M. Christoph, and I. Kirchner, ENSO variability and atmospheric response in a global coupled atmosphere-ocean GCM, *Clim. Dyn.*, *12*, 734–752, 1996.

Roeckner, E., L. Bengtsson, J. Feichter, J. Lelieveld, and H. Rodhe, Transient climate change simulations with a coupled atmosphere-ocean GCM including the tropospheric sulfur cycle, *J. Clim.*, *12*, 3004–3032, 1999.

Santer, B. D., K. E. Taylor, T. M. L. Wigley, J. E. Penner, P. D. Jones, and U. Cubasch, Towards the detection and attribution of an anthropogenic effect on climate, *Clim. Dyn.*, *12*, 77–100, 1995.

Santer, B. D., T. M. L. Wigley, T. P. Barnett, and E. Anyamba, Detection of climate change, and attribution of causes, in *Climate Change 1995: The Science of Climate Change*, edited by J. T. Houghton et al., pp. 407–443, Cambridge Univ. Press, New York, 1996a.

Santer, B. D., et al., A search for human influences on the thermal structure of the atmosphere, *Nature*, *382*, 39–46, 1996b.

Santer, B. D., J. J. Hnilo, T. M. L. Wigley, J. S. Boyle, C. Doutriaux, M. Fiorino, D. E. Parker, and K. E. Taylor, Uncertainties in observationally based estimates of temperature change in the free atmosphere, *J. Geophys. Res.*, *104*, 6305–6333, 1999.

Santer, B. D., T. M. L. Wigley, C. Doutriaux, J. S. Boyle, J. E. Hansen, P. D. Jones, G. A. Meehl, E. Roeckner, S. Sengupta, and K. E. Taylor, Accounting for the effects of volcanoes and ENSO in comparisons of modeled and observed temperature trends, *J. Geophys. Res.*, *106*, 28,033–28,059, 2001.

Seidel, D. J., R. J. Ross, J. K. Angell, and G. C. Reid, Climatological characteristics of the tropical tropopause as revealed by radiosondes, *J. Geophys. Res.*, *106*, 7857–7878, 2001.

Solomon, S., R. W. Portman, R. R. Garcia, L. W. Thomason, L. R. Poole, and M. P. McCormick, The role of aerosol variations in anthropogenic ozone depletion at northern midlatitudes, *J. Geophys. Res.*, *101*, 6713–6727, 1996.

Spencer, R. W., and J. R. Christy, Precise monitoring of global temperature trends from satellites, *Science*, *247*, 1558–1562, 1990.

Steinbrecht, W., H. Claude, U. Koehler, and K. Hoinka, Correlations between tropopause height and total ozone: Implications for long-term changes, *J. Geophys. Res.*, *103*, 19,183–19,192, 1998.

Stott, P. A., S. F. B. Tett, G. S. Jones, M. R. Allen, J. F. B. Mitchell, and G. J. Jenkins, External control of 20th century temperature by natural and anthropogenic forcings, *Science*, *290*, 2133–2137, 2000.

Tett, S. F. B., J. F. B. Mitchell, D. E. Parker, and M. R. Allen, Human influence on the atmospheric vertical temperature structure: Detection and observations, *Science*, *274*, 1170–1173, 1996.

Tett, S. F. B., P. A. Stott, M. R. Allen, W. J. Ingram, and J. F. B. Mitchell, Causes of twentieth-century temperature change near the Earth's surface, *Nature*, *399*, 569–572, 1999.

Thuburn, J., and G. C. Craig, GCM tests of theories for the height of the tropopause, *J. Atmos. Sci.*, *54*, 869–882, 1997.

Thuburn, J., and G. C. Craig, Stratospheric influence on tropopause height: The radiative constraint, *J. Atmos. Sci.*, *57*, 17–28, 2000.

Trenberth, K. E., D. P. Stepaniak, J. W. Hurrell, and M. Fiorino, Quality of reanalyses in the tropics, *J. Clim.*, *14*, 1499–1510, 2001.

Vinnikov, K. Y., A. Robock, R. J. Stouffer, J. E. Walsh, C. L. Parkinson, D. J. Cavalieri, J. F. B. Mitchell, D. Garrett, and V. F. Zakharov, Global warming and Northern Hemisphere sea ice extent, *Science*, *286*, 1934–1937, 1999.

Wang, W.-C., M. P. Dudek, X.-Z. Liang, and J. T. Kiehl, Inadequacy of effective CO_2 as a proxy in simulating the greenhouse effect of other radiatively active gases, *Nature*, *350*, 573–577, 1991.

Washington, W. M., et al., Parallel Climate Model (PCM) control and transient simulations, *Clim. Dyn.*, *16*, 755–774, 2000.

Wentz, F. J., M. Schabel, and C. Mears, Lower tropospheric air temperature derived from a blended analysis of MSU, SSM/T1, SSM/I, NCEP/NCAR reanalysis, and Reynolds SST, *Tech. Rep. 062801*, 46 pp., Remote Sens. Syst., Santa Rosa, Calif., 2001.

Wigley, T. M. L., P. J. Jaumann, B. D. Santer, and K. E. Taylor, Relative detectability of greenhouse-gas and aerosol climate change signals, *Clim. Dyn.*, *14*, 781–790, 1998.

World Meteorological Organization (WMO), Meteorology: A three-dimensional science, Second session of the commission for aerology, *WMO Bull.*, *6*(4), 134–138, 1957.

K. AchutaRao, J. S. Boyle, C. Doutriaux, B. D. Santer, and K. E. Taylor, PCMDI, Lawrence Livermore National Laboratory, P. O. Box 808, Mail Stop L-103, Livermore, CA 94550, USA. (achutarao1@llnl.gov; boyle5@llnl.gov; doutriaux1@llnl.gov; santer1@llnl.gov; taylor13@llnl.gov)

J. E. Hansen, R. Ruedy, and G. Schmidt, NASA Goddard Institute for Space Studies, 2880 Broadway, New York, NY 10025, USA. (jhansen@giss.nasa.gov; cdrar@ipcc2.giss.nasa.gov; gschmidt@giss.nasa.gov)

G. A. Meehl and T. M. L. Wigley, National Center for Atmospheric Research, 1850 Table Mesa Drive, Boulder, CO 80303, USA. (meehl@ucar.edu; wigley@ucar.edu)

E. Roeckner, Max-Planck Institute for Meteorology, D-20146 Hamburg, Germany. (roeckner@dkrz.de)

R. Sausen, Institut für Physik der Atmosphäre, Deutsches Zentrum für Luft- und Raumfahrt, Oberpfaffenhofen, D-82234 Wessling, Germany. (robert.sausen@dlr.de)